# Singularity formation in three-dimensional vortex sheets

Thomas Y. Hou[a] and Gang Hu[b]
*Applied Math, 217-50, California Institute of Technology, Pasadena, California 91125*

Pingwen Zhang[c]
*Mathematical Sciences, Peking University, Beijing 100081, China*

(Received 14 September 2001; accepted 9 October 2002; published 6 December 2002)

We study singularity formation of three-dimensional (3-D) vortex sheets without surface tension using a new approach. First, we derive a leading order approximation to the boundary integral equation governing the 3-D vortex sheet. This leading order equation captures the most singular contributions of the integral equation. By introducing an appropriate change of variables, we show that the leading order vortex sheet equation degenerates to a two-dimensional vortex sheet equation in the direction of the tangential velocity jump. This change of variables is guided by a careful analysis based on properties of certain singular integral operators, and is crucial in identifying the leading order singular behavior. Our result confirms that the tangential velocity jump is the physical driving force of the vortex sheet singularities. We also show that the singularity type of the three-dimensional problem is similar to that of the two-dimensional problem. Moreover, we introduce a model equation for 3-D vortex sheets. This model equation captures the leading order singularity structure of the full 3-D vortex sheet equation, and it can be computed efficiently using fast Fourier transform. This enables us to perform well-resolved calculations to study the generic type of 3-D vortex sheet singularities. We will provide detailed numerical results to support the analytic prediction, and to reveal the generic form of the vortex sheet singularity. © *2003 American Institute of Physics.* [DOI: 10.1063/1.1526100]

## I. INTRODUCTION

One of the classical examples of hydrodynamic instability occurs when two fluids are separated by a free surface across which the tangential velocity has a jump discontinuity. This is called Kelvin–Helmholtz instability. Kelvin–Helmholtz instability is a fundamental instability of incompressible fluid flow at high Reynolds number. The idealization of a shear layered flow as a vortex sheet separating two regions of potential flow has often been used as a model to study mixing properties, boundary layers and coherent structures of fluids. Without physical regularization such as viscosity or surface tension, the vortex sheet problem is ill-posed in the Hadamard sense. Small perturbations in high frequency modes can lead to rapid growth in time. Moreover, nonlinear interaction of high frequency modes can lead to singularity formation in finite time. It has been conjectured that Kelvin–Helmholtz instability plays a role in maintaining turbulent flow by causing the break-up of shear layers.[1]

The singularity formation in two-dimensional (2-D) vortex sheets has been thoroughly studied in the last two decades. Among the early contributions, Moore[2] studied the nonlinear evolution of a vortex sheet with a small sinusoidal initial disturbance of amplitude $\varepsilon$. He predicted that close to the singularity, the curvature of the sheet is proportional to $|\Gamma-\Gamma_s|^{-1/2}$, where $\Gamma$ is the circulation in the sheet measured from a fixed reference particle and $\Gamma_s$ is the position of the singularity. Although Moore's analysis was based on formal asymptotic analysis, his result was supported by Meiron, Baker and Orszag,[3] who analyzed a power series solution in time. Further, Moore's result was confirmed numerically by Krasny[4] and Shelley,[5] in which the roundoff error growth was controlled by spectral filtering. Moreover, as a rigorous validation of Moore's analysis, Caflisch and Orellana[6] proved the existence for a slightly perturbed vortex sheet up to $t=O(|\log(\varepsilon)|)$ for Moore's initial condition (see also Duchon and Roberts[7]). More recently, Cowley, Baker and Tanveer[8] provided a further detailed study to singularity formation of the two-dimensional vortex sheet problem. In particular, they showed how the $\frac{3}{2}$ singularity in the vortex sheet is selected at early time in the extended complex domain. Moreover, they obtained an asymptotic description of the sheet shape as the physical singularity forms.

Most studies of 2-D vortex sheets are based on formulating the problem in complex variables. Such a formulation does not generalize naturally to three-dimensional (3-D) vortex sheets. There have been only limited progresses in the study of three-dimensional vortex sheets. Among them, Ishihara and Kaneda[9] provided some evidence of the singularity formation in the three-dimensional problem by directly generalizing Moore's analysis to the three-dimensional problem. However, their result does not give a clear description of the singularity structure of the 3-D vortex sheet problem. Brady and Pullin[10] studied three-dimensional vortex sheets which have cylindrical shape and normal mode initial data. They showed that for this type of special initial data, the three-

[a]Electronic mail: hou@acm.caltech.edu
[b]Electronic mail: gang.hu@lehman.edu
[c]Electronic mail: pzhang@pku.edu.cn

 

dimensional vortex sheet problem can be reduced exactly to a two-dimensional vortex sheet problem.

In this article, we study singularity formation in three-dimensional vortex sheets with more general initial data using a new approach. We do not consider the surface tension effect in this study. The key in our analysis is to identify the leading order contribution of the three-dimensional vortex sheet equation by using properties of certain singular integral operators. This asymptotic analysis suggests a global change of variables via the Riesz transform. The leading order structure of the vortex sheet problem becomes more apparent using the new variables. Moreover, the leading order asymptotic analysis suggests we use the dipole strength as one of the independent variables. Using these new variables, we obtain a surprising result: along the direction of the tangential velocity jump, the three-dimensional vortex sheet problem can be effectively reduced to a corresponding two-dimensional problem to the leading order approximation. More precisely, we show that the Kelvin–Helmholtz instability is mainly due to the coupling of two of the three transformed interface variables. The analysis also suggests that one need only to complexify one of the two independent variables along the direction of the tangential velocity jump. The other independent variable serves as a parametrization of the singularity curve in the extended complex domain. Thus many techniques for studying singularity formation for 2-D vortex sheets can be used to study singularity formation for 3-D vortex sheets.

What is the generic form of vortex sheet singularities in 3-D vortex sheets? We investigate this question by studying the early time singularity formation of solutions to the three-dimensional vortex sheet equations. The key in studying the early time singularity is to derive a local approximate system for the vortex sheet equations. Previous studies (see Moore,[2,11] Caflisch and Semmes,[12] Cowley, Baker and Tanveer[8]) relied on complexifying the integral and applying the residue theorem. However, there is no natural way to extend this idea to the three-dimensional problem. Here we take a different approach which applies to the three-dimensional problem. By using the dipole representation and Bernoulli's equation, we are able to derive the local terms describing the velocity jump in the tangential directions across the sheet. From this local approximate system, we show that along certain space curves on the three-dimensional vortex sheet surface, singularity formation is equivalent to that of a two-dimensional vortex sheet to the leading order. Moreover, by choosing a special set of coordinates at $t=0$ and complexifying one of the two independent variables, we show that branch point singularities of order 3/2 develop spontaneously at $t=0+$ in the extended complex domain. The formation of the complex singularity of order 3/2 at $t=0+$ from initially analytic data is a singular perturbation in time due to the strong nonlinear interaction. Once the 3/2 singularity is formed, it generically does not change type dynamically, and it becomes a physical singularity when it reaches the real axis.

To study the local form of the curvature singularity at the physical singularity time, we employ the asymptotic analysis performed by Hou and Zhang.[13] We present an approximation to the local vortex sheet surface in the neighborhood of the singularity near the physical singularity time. We show that with an appropriate transformation of the interface variables, the local form of the curvature singularity is observed only in two of the three components to the leading order. Thus, the technique used by Cowley, Baker and Tanveer[8] can be applied to obtain the local form of the singularity at the singularity time. We remark that the leading order asymptotic analysis cannot determine the order of the singularity. This information must be obtained from the early time singularity analysis using a singular perturbation technique. The analysis needs to takes into account the nonlinear interactions among various singular terms by appropriately rescaling the space and time variables near the singularity.

One interesting open question is whether the singularity in a 3-D vortex sheet first appears as isolated points or along a one-dimensional line segment? We investigate this question in our paper. By studying the motion of singularities in the extended complex domain, we show that the singularity curve in the extended complex domain is actually an analytic function of its parametrization $\beta_2$ (see Sec. III C). Using analytic continuation, we argue that when physical singularities form, they appear either at some isolated points, or along the entire one-dimensional curve in the real parameter plane. It is not possible for the interface to develop finite time singularities along a segment of a one-dimensional curve.

To confirm our analytical study, we perform careful numerical experiments to study singularity formation in 3-D vortex sheets. However, direct simulations of the three-dimensional vortex sheet equations are very expensive. The complexity in every time step is $O(N^4)$ by direct summations of the dipole representation, where $N$ is the number of particles used to discretize the surface in each dimension. Moreover, for initial conditions which are double periodic perturbations to the flat surface, one has to sum the contributions from all the periodic images. This adds substantially to the overall computational cost. It becomes prohibitively expensive even with $N$ at the level of $O(100)$. The fast multipole methods developed by Greengard and Rokhlin,[14] Berman and Greengard[15] can be used in principle to reduce the operating account to $cN^2$. However, the constant $c$ could be quite large in practice.

To alleviate the numerical difficulty mentioned above, we introduce a model equation for the three-dimensional vortex sheet problem. Our model equation has two important properties. First, it captures the leading order behavior of the singular solution of 3-D vortex sheets. In fact, we show that our model equation forms the same tangential velocity jump as that of the full equation. Therefore, by applying the same analysis developed for the full equation, we can show that our model equation captures the same singularity type of the full equation. We also show that the local singularity structure of our model equation has the same form as that of the full equation near the physical singularity time. Another important property of our model equation is that it can be computed efficiently. In particular, we show that when using a special coordinate, our model equation can be expressed in terms of certain Riesz transforms, which are convolution operators. Thus our model equation can be evaluated with the

fast Fourier transform (FFT) with $O(N^2 \log(N))$ operation count. This offers a tremendous saving over the full equation and enables us to perform well-resolved computations to study the singularity formation of 3-D vortex sheets. Our extensive numerical study provides partial confirmation of our analytical predictions. In particular, our results show that the three-dimensional vortex sheet develops a curvature singularity in finite time. We provide evidence showing that the singularity is of order 3/2, and the singularity is essentially two-dimensional.

The rest of the paper is organized as follows. In Sec. II, we review the formulation of 3-D vortex sheets and derive the leading order approximation to the 3-D vortex sheet. In Sec. III, we study the early time singularity formation and the local singularity form in the three-dimensional vortex sheet problem. Our model equation is introduced and analyzed by similar asymptotic analysis in Sec. IV. We devote Sec. V to the numerical study of singularity formation using the model equation.

## II. FORMULATION AND LEADING ORDER ANALYSIS

In this section, we first review the formulation of the 3-D vortex sheet problem. We then apply a leading order analysis to the 3-D vortex sheet equation near the equilibrium state. This leading order analysis provides a critical guideline to our study of singularity formation in 3-D vortex sheets. The analysis is based on properties of certain singular integral operators. Using a special transformation of the interface variables, we show that the 3-D vortex sheet problem is essentially equivalent to a 2-D vortex sheet problem. Furthermore, our analysis indicates that the tangential velocity jump between the upper and lower layer of the fluid is the driving force of the instability.

### A. Formulation of the 3-D vortex sheet equation

We consider an interface $\Gamma$ separating two infinite layers of incompressible, inviscid, irrotational and identical fluids in the absence of surface tension. Under the Lagrangian frame, the interface location at any instant $t$ is in the form of

$$\mathbf{z}(\alpha_1,\alpha_2,t)=(x(\alpha_1,\alpha_2,t),y(\alpha_1,\alpha_2,t),z(\alpha_1,\alpha_2,t))^T, \tag{1}$$

where $(\alpha_1,\alpha_2)$ is the Lagrangian surface parameter. Thus, the normalized tangential vectors to the surface, $\mathbf{t}_1$ and $\mathbf{t}_2$, are defined by

$$\mathbf{t}_1=\frac{\mathbf{z}_{\alpha_1}}{|\mathbf{z}_{\alpha_1}|}, \quad \mathbf{t}_2=\frac{\mathbf{z}_{\alpha_2}}{|\mathbf{z}_{\alpha_2}|}. \tag{2}$$

The unit normal vector to the surface $\mathbf{n}$ is defined by

$$\mathbf{n}=\frac{\mathbf{z}_{\alpha_1}\times\mathbf{z}_{\alpha_2}}{|\mathbf{z}_{\alpha_1}\times\mathbf{z}_{\alpha_2}|}. \tag{3}$$

We label the region below the interface as Region 1 and the region above the interface as Region 2. Under this notation, the velocity field $\mathbf{u}_1$ ($\mathbf{u}_2$) is the velocity below (above) the interface. We define $\mathbf{u}_+$ to be the limit of $\mathbf{u}_2$ approaching the interface from Region 2 and $\mathbf{u}_-$ to be the limit of $\mathbf{u}_1$ approaching the interface from Region 1. Since the flow in each region is irrotational, we can introduce the velocity potentials $\phi_1$ and $\phi_2$ so that

$$\mathbf{u}_1=\nabla\phi_1, \quad \mathbf{u}_2=\nabla\phi_2. \tag{4}$$

Furthermore, since the flows are incompressible in their respective regions, the velocity potentials satisfy the Laplace equation:

$$\nabla^2\phi_1=0 \quad \text{and} \quad \nabla^2\phi_2=0.$$

We express the potentials in the fluid domain using a dipole representation:[16]

$$\phi(\mathbf{z})=\int \mu(\alpha')(\mathbf{z}_{\alpha_1}\times\mathbf{z}_{\alpha_2})(\alpha')\cdot\nabla_{z'}G(\mathbf{z}-\mathbf{z}(\alpha'))d\alpha', \tag{5}$$

where $\alpha'=(\alpha_1',\alpha_2')$ and

$$G(\mathbf{z}-\mathbf{z}')=-\frac{1}{4\pi|\mathbf{z}-\mathbf{z}'|},$$

$$\nabla_{z'}G(\mathbf{z}-\mathbf{z}')=-\frac{\mathbf{z}-\mathbf{z}'}{4\pi|\mathbf{z}-\mathbf{z}'|^3},$$

and $\mu(\alpha)=\phi_- - \phi_+$. Here $\phi_-$ and $\phi_+$ are the potentials approaching the interface from Region 2 and Region 1, respectively.

After differentiating Eq. (5) with respect to $\mathbf{z}$ and then integrating by parts, we obtain

$$\nabla\phi(\mathbf{z})=\int |\nabla_\alpha\mu(\alpha')^T,\nabla_\alpha\mathbf{z}(\alpha')^T|\times\nabla_{\mathbf{z}'}G(\mathbf{z}-\mathbf{z}(\alpha'))\,d\alpha', \tag{6}$$

where we have used the notation

$$|\nabla_\alpha\mu(\alpha')^T,\nabla_\alpha\mathbf{z}(\alpha')^T|=\frac{\partial\mu}{\partial\alpha_1}\mathbf{z}_{\alpha_2}-\frac{\partial\mu}{\partial\alpha_2}\mathbf{z}_{\alpha_1}.$$

In the Lagrangian formulation of the interface problem, the motion of the interface is governed by

$$\frac{\partial\mathbf{z}(\alpha,t)}{\partial t}=\mathbf{u}(\mathbf{z}(\alpha,t),t), \quad \mathbf{z}(\alpha,0)=\mathbf{z}_0(\alpha),$$

where $\mathbf{u}=(u,v,w)$ is the velocity of fluid particles on the interface. The kinematic condition that ensures the interface moving with the fluid requires the normal component of the velocity to be continuous at the interface. However, the tangential velocity at the interface is arbitrary and we choose it at our convenience.

For the vortex sheet problem, we apply Bernoulli's equation to the upper and lower layer of fluid, respectively. Using the continuity of the normal stress and Eqs. (5)–(6), one can show that by choosing the interface velocity to be the average of the interface velocity from above $\mathbf{u}_+$ and the interface velocity from below $\mathbf{u}_-$ from above and from below, respectively, i.e., $\mathbf{u}=\frac{1}{2}(\mathbf{u}_+ + \mathbf{u}_-)$, then we have[17]

$$\frac{\partial\mu}{\partial t}(\alpha,t)=0. \tag{7}$$

Equation (7) says that the circulation stays constant along the trajectories whose motions are determined by the average fluid velocity.

With this particular choice of tangential velocity, the velocity of the vortex sheet interface can be obtained by the average of the limiting velocities in Eq. (6) approaching from the upper and lower layer of fluid. The equation of the surface particle motion can be written as[18]

$$\frac{\partial \mathbf{z}}{\partial t}(\alpha,t)=\int |\nabla_\alpha \mu(\alpha')^T, \nabla_\alpha \mathbf{z}(\alpha',t)^T| \times \nabla_{\mathbf{z}'} G(\mathbf{z}(\alpha,t) - \mathbf{z}(\alpha',t))\, d\alpha', \tag{8}$$

$$\mathbf{z}(\alpha,0)=\mathbf{z}_0(\alpha), \tag{9}$$

where the integral takes the Cauchy principal value.

Sometimes it is more convenient to use a different set of parametrization $(\beta_1,\beta_2)$ for the vortex sheet in our analysis. Except in Secs. III C and IV B, this change of parametrization is made at a fixed time and is time independent. Thus $\beta$ is still a Lagrangian variable. We remark that it is essential to perform our analysis of 3-D vortex sheet singularities in the Lagrangian frame. The Lagrangian formulation contains some important physical information about the singularity formation. The change of variables from $\alpha$ to $\beta$ enables us to obtain a simplified leading order system and reveal the two-dimensional nature of the three-dimensional vortex sheet problem.

When the change of parametrization is time dependent, as in Sec. III C and Sec. V B, the vortex sheet equation needs to be modified by adding an appropriate tangential velocity field:

$$\frac{\partial \mathbf{z}}{\partial t}(\beta,t)=\int |\nabla_\beta \mu(\beta')^T, \nabla_\beta \mathbf{z}(\beta',t)^T| \times \nabla_{\mathbf{z}'} G(\mathbf{z}(\beta,t) - \mathbf{z}(\beta',t))\, d\beta' + T^1 \mathbf{t}_1 + T^2 \mathbf{t}_2, \tag{10}$$

$$\frac{\partial \mu}{\partial t}(\beta,t)=\frac{T^1}{|\mathbf{z}_{\beta_1}|}\mu_{\beta_1}+\frac{T^2}{|\mathbf{z}_{\beta_2}|}\mu_{\beta_2}. \tag{11}$$

$T^1$ and $T^2$ are the added tangential velocities to the vortex sheet. By choosing $T^1$ and $T^2$ properly, we can impose a certain special property of the parametrization for the vortex sheet. Note that the shape of the vortex sheet is solely determined by the normal velocity. The tangential velocity of the interface only changes the paremetrization of the vortex sheet, but not the shape of the interface.

It is tempting to perform the analysis of vortex sheet singularities in a non-Lagrangian dynamic new frame. However, this would lose certain essential features that come with the Lagrangian frame and complicate the analysis considerably. We only deal with the effect of a dynamical change of variables when it is necessary, e.g., when we discuss the motion of complex singularities and the numerical computations.

### B. Leading order analysis of the near-equilibrium case

In this subsection, we perform leading order analysis of for the vortex sheet equation (8) near equilibrium. This asymptotic analysis provides the critical leading order structure of the 3-D vortex sheet equation. It reveals the surprising two-dimensional nature of the three-dimensional vortex sheet problem under appropriate changes of variables. In particular, the analysis in this section suggests the global change of variables for the interface position using the Riesz transform. A variant of this change of variables will be used in Sec. III D when we study the structure of the physical singularity. The analysis in this section also suggests the change of variable from the original Lagrangian variable, $\alpha$, to $\beta$, by introducing the dipole strength, $\mu$, as one of the independent Lagrangian variables. A variant of this change of variables plays an essential role in our analysis of early time singularity formation in Sec. III B.

The leading order approximation is obtained by performing asymptotic analysis for vortex sheets near equilibrium. First, we express the interface variable $\mathbf{z}$ in the form of

$$\mathbf{z}=\begin{pmatrix} x \\ y \\ z \end{pmatrix}=\begin{pmatrix} \alpha_1 \\ \alpha_2 \\ 0 \end{pmatrix}+\begin{pmatrix} S_1 \\ S_2 \\ S_3 \end{pmatrix}, \tag{12}$$

where $S_1$, $S_2$ and $S_3$ are small in amplitude and are double periodic with period of $(2\pi\times 2\pi)$. Under this assumption, Eq. (8) in the original Lagrangian parametrization becomes

$$\begin{aligned}\frac{\partial \mathbf{z}}{\partial t} &= -\frac{1}{4\pi}\int\int \frac{(\gamma_1 \mathbf{z}'_{\alpha_2}-\gamma_2 \mathbf{z}'_{\alpha_1})\times(\mathbf{z}-\mathbf{z}')}{|\mathbf{z}-\mathbf{z}'|^3}\, d\mathbf{z}' \\ &= -\frac{1}{4\pi}\int\int \left[ \gamma_1 \begin{pmatrix} S'_{1\alpha_2} \\ 1+S'_{2\alpha_2} \\ S'_{3\alpha_2} \end{pmatrix} - \gamma_2 \begin{pmatrix} 1+S'_{1\alpha_1} \\ S'_{2\alpha_1} \\ S'_{3\alpha_1} \end{pmatrix} \right] \\ &\quad \times \begin{pmatrix} \alpha_1-\alpha'_1+S_1-S'_1 \\ \alpha_2-\alpha'_2+S_2-S'_2 \\ S_3-S'_3 \end{pmatrix} \frac{d\alpha'}{|\mathbf{z}-\mathbf{z}'|^3},\end{aligned}$$

where $\gamma_i=\partial\mu/\partial\alpha_i$ $(i=1,2)$, $\mathbf{z}'=\mathbf{z}(\alpha',t)$ and $S'_i=S_i(\alpha',t)$ $(i=1,2,3)$. We assume that the amplitude of $S_i$ is of order $\varepsilon$, i.e., $S_i\sim O(\varepsilon)$, and assume that $\gamma_i$ is of order $\varepsilon$ perturbation to a constant vortex sheet strength. It is reasonable to consider the linear terms in the numerator of the integral as the leading order terms. By writing down every component separately and keeping only the linear terms in the numerator of the integrand, we obtain approximate equations for $S_1$, $S_2$ and $S_3$ as follows:

$$\frac{\partial S_1}{\partial t}=-\frac{1}{4\pi}\int\int\frac{(\gamma_1(1+S'_{2\alpha_2})-\gamma_2 S'_{2\alpha_1})(S_3-S'_3)}{|z-\mathbf{z}'|^3}-\frac{(\gamma_1 S'_{3\alpha_2}-\gamma_2 S'_{3\alpha_1})(\alpha_2-\alpha'_2+S_2-S'_2)}{|\mathbf{z}-\mathbf{z}'|^3}d\alpha'$$

$$=-\frac{1}{4\pi}\int\int\frac{\gamma_1(S_3-S'_3)-(\gamma_1 S'_{3\alpha_2}-\gamma_2 S'_{3\alpha_1})(\alpha_2-\alpha'_2)}{|\mathbf{z}-\mathbf{z}'|^3}d\alpha'+O(\varepsilon^2), \tag{13}$$

$$\frac{\partial S_2}{\partial t}=-\frac{1}{4\pi}\int\int\frac{(\gamma_1 S'_{3\alpha_2}-\gamma_2 S'_{3\alpha_1})(\alpha_1-\alpha'_1+S_1-S'_1)}{|\mathbf{z}-\mathbf{z}'|^3}-\frac{(\gamma_1 S'_{1\alpha_2}-\gamma_2(1+S'_{1\alpha_1}))(S_3-S'_3)}{|\mathbf{z}-\mathbf{z}'|^3}d\alpha'$$

$$=-1.5q\frac{1}{4\pi}\int\int\frac{\gamma_2(S_3-S'_3)+(\gamma_1 S'_{3\alpha 2}-\gamma_2 S'_{3\alpha_1})(\alpha_1-\alpha'_1)}{|\mathbf{z}-\mathbf{z}'|^3}d\alpha'+O(\varepsilon^2), \tag{14}$$

and

$$\frac{\partial S_3}{\partial t}=-\frac{1}{4\pi}\int\int\frac{(\gamma_1 S'_{1\alpha_2}-\gamma_2(1+S'_{1\alpha_1}))(\alpha_2-\alpha'_2+S_2-S'_2)}{|\mathbf{z}-\mathbf{z}'|^3}-\frac{(\gamma_1(1+S'_{2\alpha_2})-\gamma_2 S'_{2\alpha_1})(\alpha_1-\alpha'_1+S_1-S'_1)}{|\mathbf{z}-\mathbf{z}'|^3}d\alpha'$$

$$=-\frac{1}{4\pi}\int\int\frac{(\gamma_1 S'_{1\alpha_2}-\gamma_2 S'_{1\alpha_1})(\alpha_2-\alpha'_2)}{|\mathbf{z}-\mathbf{z}'|^3}-\frac{(\gamma_1 S'_{2\alpha_2}-\gamma_2 S'_{2\alpha_1})(\alpha_1-\alpha'_1)}{|\mathbf{z}-\mathbf{z}'|^3}$$

$$-\frac{\gamma_1(\alpha_1-\alpha'_1+S_1-S'_1)+\gamma_2(\alpha_2-\alpha'_2+S_2-S'_2)}{|\mathbf{z}-\mathbf{z}'|^3}d\alpha'+O(\varepsilon^2), \tag{15}$$

where we have used the notations $\mathbf{z}=\mathbf{z}(\alpha)$, $\mathbf{z}'=\mathbf{z}(\alpha')$ and $S_j=S_j(\alpha)$, $S'_j=S_j(\alpha')$, $j=1,2,3$.

Recall that to the leading order, we have

$$|\mathbf{z}-\mathbf{z}'|\approx|\alpha-\alpha'|.$$

Thus the above integral equations can be expressed in terms of the Riesz transforms which are defined as follows:

$$H_i(f)=\frac{1}{2\pi}\int\int\frac{(\alpha_i-\alpha'_i)f(\alpha')}{[(\alpha_1-\alpha'_1)^2+(\alpha_2-\alpha'_2)^2]^{3/2}}d\alpha',\quad i=1,2, \tag{16}$$

$$\Lambda(f)=\frac{1}{2\pi}\int\int\frac{f(\alpha)-f(\alpha')}{[(\alpha_1-\alpha'_1)^2+(\alpha_2-\alpha'_2)^2]^{3/2}}d\alpha', \tag{17}$$

for $f\in L^p(R^2)$, where $1<p<\infty$. The integrals take the Cauchy principal value. It is well-known that the Riesz transforms satisfy the following properties:[19]

$$H_1^2+H_2^2=-I,\quad H_1D_1+H_2D_2=\Lambda, \tag{18}$$

$$\Lambda H_i=-D_i,\quad H_1D_2=H_2D_1,\quad i=1,2, \tag{19}$$

for functions with zero mean, i.e., $\int f(\alpha)d\alpha=0$, where $D_i=\partial_{\alpha_i}$ is the partial derivative with respect to $\alpha_i$. The above properties can be verified easily from the spectral symbols of the Riesz transforms:[19]

$$\widehat{H_kf}=\frac{-i\xi_k}{(\xi_1^2+\xi_2^2)^{1/2}}\hat{f},\quad k=1,2, \tag{20}$$

$$\widehat{\Lambda f}=(\xi_1^2+\xi_2^2)^{1/2}\hat{f}, \tag{21}$$

in which $\hat{f}$ stands for the Fourier transformation of $f$.

From these properties, we find some surprising cancellations when the problem is projected in certain variables, and the leading order problem becomes essentially a two-dimensional problem. Guided by the properties of the Riesz transform, we introduce the following change of variables:

$$\psi_1=H_2(S_1)-H_1(S_2), \tag{22}$$

$$\psi_2=H_1(S_1)+H_2(S_2), \tag{23}$$

$$\psi_3=S_3. \tag{24}$$

Using (18)–(19), we can also express $(S_1,S_2,S_3)$ in terms of $(\psi_1,\psi_2,\psi_3)$ through the following equations:

$$S_1=-H_2(\psi_1)-H_1(\psi_2)+\langle S_1\rangle, \tag{25}$$

$$S_2=H_1(\psi_1)-H_2(\psi_2)+\langle S_2\rangle, \tag{26}$$

$$S_3=\psi_3 \tag{27}$$

where $\langle S_i\rangle=1/4\pi^2\int_{-\pi}^{\pi}\int_{-\pi}^{\pi}S_i(\alpha)d\alpha$, $i=1,2$.

Differentiating Eqs. (22) and (23) with respect to time $t$, we have

$$\frac{\partial\psi_1}{\partial t}=H_2\left(\frac{\partial S_1}{\partial t}\right)-H_1\left(\frac{\partial S_2}{\partial t}\right), \tag{28}$$

$$\frac{\partial\psi_2}{\partial t}=H_1\left(\frac{\partial S_1}{\partial t}\right)+H_2\left(\frac{\partial S_2}{\partial t}\right). \tag{29}$$

To derive the leading order terms of the evolution equation for $\psi_1$, we substitute (13) and (14) into (28). The result is

$$\frac{\partial \psi_1}{\partial t} = H_2\left(\frac{\partial S_1}{\partial t}\right) - H_1\left(\frac{\partial S_2}{\partial t}\right)$$
$$= H_2\left( -\frac{1}{4\pi}\int \frac{\gamma_1(S_3 - S_3') - (\gamma_1 S'_{3\alpha_2} - \gamma_2 S'_{3\alpha_1})(\alpha_2 - \alpha_2')}{|\mathbf{z}-\mathbf{z}'|^3} d\alpha' \right)$$
$$- H_1\left( -\frac{1}{4\pi}\int \frac{\gamma_2(S_3 - S_3') + (\gamma_1 S'_{3\alpha_2} - \gamma_2 S'_{3\alpha_1})(\alpha_1 - \alpha_1')}{|\mathbf{z}-\mathbf{z}'|^3} d\alpha' \right) + O(\varepsilon^2). \tag{30}$$

Note that given $\mathbf{z}$ in the form of (12), we have

$$|\mathbf{z}-\mathbf{z}'| = |\alpha - \alpha'| + O(\varepsilon). \tag{31}$$

Thus the denominator of the vortex sheet kernel can be approximated by that of the Riesz transform kernel. With this observation, we can show that

$$\frac{\partial \psi_1}{\partial t} = -\frac{1}{2} H_2(\gamma_1 \Lambda S_3 - \gamma_1 H_2 D_2 S_3 + \gamma_2 H_2 D_1 S_3)$$
$$+ \frac{1}{2} H_1(\gamma_2 \Lambda S_3 + \gamma_1 H_1 D_2 S_3 - \gamma_2 H_1 D_1 S_3) + O(\varepsilon^2)$$
$$= -\frac{1}{2} H_2(\gamma_1 H_1 D_1 S_3 + \gamma_2 H_2 D_1 S_3)$$
$$+ \frac{1}{2} H_1(\gamma_1 H_1 D_2 S_3 + \gamma_2 H_2 D_2 S_3) + O(\varepsilon^2) = O(\varepsilon^2), \tag{32}$$

where we have used the properties of the Riesz transforms (18)–(19) in the last step. As we can see, the Kelvin–Helmholtz instability is eliminated to the leading order in the $\psi_1$ variable. In Sec. III D, we will use a similar analysis to study the structure of curvature singularity at the physical singularity time. The fact that the $\psi_1$ variable can be eliminated from the leading order approximation plays an essential role in obtaining a close form approximation of the leading order curvature singularity structure.

Similarly, to derive the leading order terms in the evolution equation of $\psi_2$, we substitute (13) and (14) into (29) and get

$$\frac{\partial \psi_2}{\partial t} = H_1\left(\frac{\partial S_1}{\partial t}\right) + H_2\left(\frac{\partial S_2}{\partial t}\right)$$
$$= -\frac{1}{2} H_1(\gamma_1 \Lambda S_3 - \gamma_1 H_2 D_2 S_3 + \gamma_2 H_2 D_1 S_3)$$
$$- \frac{1}{2} H_2(\gamma_2 \Lambda S_3 + \gamma_1 H_1 D_2 S_3 - \gamma_2 H_1 D_1 S_3) + O(\varepsilon^2)$$
$$= -\frac{1}{2} H_1(\gamma_1 H_1 D_1 S_3 + \gamma_2 H_2 D_1 S_3)$$
$$- \frac{1}{2} H_2(\gamma_1 H_1 D_2 S_3 + \gamma_2 H_2 D_2 S_3) + O(\varepsilon^2). \tag{33}$$

Applying the properties of the Riesz transforms (18)–(19) one more time, we can further reduce the above equation to

$$\frac{\partial \psi_2}{\partial t} = -\frac{1}{2}\gamma_1 D_1 (H_1 H_1 + H_2 H_2) S_3$$
$$- \frac{1}{2}\gamma_2 D_2 (H_1 H_1 + H_2 H_2) S_3 + O(\varepsilon^2)$$
$$= \frac{1}{2}(\gamma_1 D_1 + \gamma_2 D_2) S_3 + O(\varepsilon^2). \tag{34}$$

The derivation of the leading order evolution equation for $\psi_3$ is more involved. We will leave the detailed derivation to Appendix A. After some manipulations, we can show that the leading order equation for $\psi_3$ is given by

$$\frac{\partial \psi_3}{\partial t} = -\frac{1}{2}(\gamma_1 D_1 + \gamma_2 D_2)\psi_2 + \frac{1}{2}(\gamma_2 D_1 - \gamma_1 D_2)\psi_1$$
$$+ O(\varepsilon^2). \tag{35}$$

Combining (13), (14) and (35) into a system, we get

$$\frac{\partial \psi_1}{\partial t} = O(\varepsilon^2), \tag{36}$$

$$\frac{\partial \psi_2}{\partial t} = \frac{1}{2}(\gamma_1 D_1 + \gamma_2 D_2)\psi_3 + O(\varepsilon^2), \tag{37}$$

$$\frac{\partial \psi_3}{\partial t} = -\frac{1}{2}(\gamma_1 D_1 + \gamma_2 D_2)\psi_2 + \frac{1}{2}(\gamma_2 D_1 - \gamma_1 D_2)\psi_1$$
$$+ O(\varepsilon^2), \tag{38}$$

where $D_1$ ($D_2$) stands for differentiation with respect to the $\alpha_1$ ($\alpha_2$) variable. The above leading order system is consistent with the leading order linearized system derived in the article of Hou and Zhang.[13]

Recall that $\gamma_i = \partial\mu/\partial\alpha_i$, $i = 1,2$. The above leading order analysis suggests a natural change of variables from $\alpha$ to $\beta$ as follows:

$$\beta_1 = \mu(\alpha_1, \alpha_2), \tag{39}$$

$$\beta_2 = \int_{(0,0)}^{(\alpha_1,\alpha_2)} \mu_{\alpha_2}(\alpha_1', \alpha_2') d\alpha_1' - \mu_{\alpha_1}(\alpha_1', \alpha_2') d\alpha_2'. \tag{40}$$

The integration in (40) is path independent since $(\mu_{\alpha_2}, -\mu_{\alpha_1})$ is divergence free.

Note that through this change of variables, we use the dipole strength as one of the independent variables. The dipole strength variable corresponds to the vortex line direction $(\gamma_1, \gamma_2)$. Thus, this choice of coordinates has a natural physical interpretation. On the other hand, the $\beta_2$ variable corresponds to the direction that is orthogonal to the vortex

line direction. It is the parametrization of the level set $\mu = \beta_1$ for a constant value of $\beta_1$. The idea of introducing $\mu$ as one of the independent variables motivates the change of variables introduced in Secs. III A and III D. It plays an essential role in understanding the early time singularity structure and the curvature singularity at the physical singularity time. We remark that the above change of variables in the parametrization is time independent since $\mu(\alpha)$ is time independent. Thus, there is no induced tangential velocity field produced through this change of variables.

Substituting this change of variables into system (36)–(38), we obtain

$$\frac{\partial \psi_1}{\partial t} = O(\varepsilon^2), \tag{41}$$

$$\frac{\partial \psi_2}{\partial t} = \frac{1}{2} D_{\beta_1} \psi_3 + O(\varepsilon^2), \tag{42}$$

$$\frac{\partial \psi_3}{\partial t} = -\frac{1}{2} D_{\beta_1} \psi_2 + \frac{1}{2} D_{\beta_2} \psi_1 + O(\varepsilon^2). \tag{43}$$

In the new coordinates, we can see that the system suffers the Kelvin–Helmholtz instability because of the coupling of (42) and (43). It also shows that the $\beta_1$ direction is the unstable direction responsible for generating Kelvin–Helmholtz instability. Moreover, since the $\beta_1$ direction is the tangential velocity jump direction between the upper and lower layers of fluid, the leading order terms confirm that the tangential velocity jump is the physical driving force of the instability of the three-dimensional vortex sheet.

In a separate article,[20] Hou and Hu prove a nearly optimal existence result for 3-D vortex sheets based on the above system. In particular, they prove rigorously that the $O(\varepsilon^2)$ terms are in fact smaller or smoother than the leading order terms. In this article, we focus on the analysis of the singularity structure. Equations (41), (42) and (43) provide us with a critical insight on the singularity structure. This will become clear in the study presented in the next section.

## III. EARLY TIME SINGULARITY FORMATION

Following the leading order analysis from the last section, we study the early time singularity formation in this section. The study of the early time singularity formation is important because it reveals the mechanism why a branch point singularity of order 3/2 is selected generically at $t = 0+$ in the extended complex domain from the initial analytic solution. This selection mechanism is a result of the strong nonlinear interaction of the leading order system in the extended complex domain. Once the initial singularity is formed, it will propagate in time along certain smooth characteristics without changing its type. The analysis is based on a singular perturbation expansion in time around certain singular points related to the derivatives of the Lagrangian interface position in the extended complex domain.

Our work is motivated by a related study of Cowley, Baker and Tanveer[8] for 2-D vortex sheets. The key in their approach is to derive a leading order *local* system and to extend the interface variable to a complex domain. Variants of such local system have also been derived and studied by other researchers (see Moore,[2] Caflisch and Semmes[12]). In most previous studies, the leading order local system was derived by means of a complex analysis. A special feature of the two-dimensional vortex sheet problem is that one can combine $x$ and $y$ to form a complex variable $z(\alpha) = x(\alpha) + iy(\alpha)$, and further complexify $\alpha$ to treat $z$ as an analytic function. This idea has no obvious extension to the three-dimensional problem.

### A. Early time singularities in 3-D vortex sheets

In this subsection, we derive a local approximate system to the 3-D vortex sheet equation using a different approach. Our derivation is based on the observation that the tangential velocity difference is the driving force of the Kelvin–Helmholtz instability. This is the common feature between the two- and the three-dimensional problems. In fact, we can re-derive the local approximate system for 2-D vortex sheets using the same approach.

By combining the dipole formulation with the vorticity formulation, Haroldsen and Meiron[18] have derived the velocity on the interface. In particular, using Eq. (6) related to the upper layer fluid, one can obtain the interface velocity $V(\alpha,t)$ as

$$V(\alpha,t) = \nabla \phi(\mathbf{z}(\alpha,t),t) = -V_{\mathrm{loc}}(\alpha,t) + V_1(\alpha,t), \tag{44}$$

where

$$V_1(\alpha,t) = \lim_{\substack{\mathbf{z}\to\mathbf{z}(\alpha,t) \\ \text{from upper layer}}} \int |\nabla_\alpha \mu(\alpha')^T, \nabla_\alpha \mathbf{z}(\alpha',t)^T| \times \nabla_{z'} G(\mathbf{z} - \mathbf{z}(\alpha',t)) d\alpha', \tag{45}$$

$$V_{\mathrm{loc}}(\alpha,t) = \frac{1}{2} |\nabla_\alpha \mu(\alpha')^T, \nabla_\alpha \mathbf{z}(\alpha',t)^T| \times \frac{\mathbf{z}_{\alpha_1} \times \mathbf{z}_{\alpha_2}}{|\mathbf{z}_{\alpha_1} \times \mathbf{z}_{\alpha_2}|^2}(\alpha,t). \tag{46}$$

Similarly, using the equation related to the lower layer fluid, we get

$$V(\alpha,t) = \nabla \phi(\mathbf{z}(\alpha),t) = V_{\mathrm{loc}}(\alpha,t) + V_2(\alpha,t), \tag{47}$$

where

$$V_2(\alpha,t) = \lim_{\substack{\mathbf{z}\to\mathbf{z}(\alpha,t) \\ \text{from lower layer}}} \int |\nabla_\alpha \mu(\alpha')^T, \nabla_\alpha \mathbf{z}(\alpha',t)^T| \times \nabla_{z'} G(\mathbf{z} - \mathbf{z}(\alpha',t)) d\alpha'. \tag{48}$$

We note that $V(\alpha,t) = \frac{1}{2}(V_1(\alpha,t) + V_2(\alpha,t))$.

Further, we choose a parametrization $\alpha$ at $t = 0$ such that the coordinate satisfies

$$\mathbf{z}_{\alpha_1} \cdot \mathbf{z}_{\alpha_2} = 0, \tag{49}$$

$$\frac{\partial \mu}{\partial \alpha_1} = 1, \quad \frac{\partial \mu}{\partial \alpha_2} = 0, \tag{50}$$

at time $t=0$. In some sense, we use the dipole strength $\mu$ as one of the independent variables. As we will see later, this gives rise to a natural interpretation of the Kelvin–Helmholtz instability. We remark that this is not a strong assumption. In fact, we can show that starting from a given coordinate, we can find a coordinate that satisfies (49) and (50). We defer the justification of such coordinate to the next subsection.

Using the properties (49) and (50), we can simplify the local term to

$$V_{\text{loc}}=\frac{1}{2}|\nabla_\alpha \mu^T, \nabla_\alpha \mathbf{z}^T| \times \frac{\mathbf{z}_{\alpha_1}\times \mathbf{z}_{\alpha_2}}{|\mathbf{z}_{\alpha_1}\times \mathbf{z}_{\alpha_2}|^2}$$

$$=\frac{1}{2}\mathbf{z}_{\alpha_2}\times \frac{\mathbf{z}_{\alpha_1}\times \mathbf{z}_{\alpha_2}}{|\mathbf{z}_{\alpha_1}\times \mathbf{z}_{\alpha_2}|^2}$$

$$=\frac{\mathbf{z}_{\alpha_1}}{2|\mathbf{z}_{\alpha_1}|^2}. \tag{51}$$

Thus, substituting (51) into Eqs. (44) and (47), we can express the evolution equation for the 3-D vortex sheet in the following two equivalent formulations:

$$\frac{\partial \mathbf{z}(\alpha,t)}{\partial t}=-\frac{\mathbf{z}_{\alpha_1}(\alpha,t)}{2|\mathbf{z}_{\alpha_1}(\alpha,t)|^2}+V_1(\alpha,t), \tag{52}$$

$$\frac{\partial \mathbf{z}(\alpha,t)}{\partial t}=\frac{\mathbf{z}_{\alpha_1}(\alpha,t)}{2|\mathbf{z}_{\alpha_1}(\alpha,t)|^2}+V_2(\alpha,t), \tag{53}$$

at $t=0$, where $V_1$ and $V_2$ are defined in (45) and (48).

To derive our local approximate system for 3-D vortex sheets, we use the Clifford algebra (see also Wu[21]). Let $e_1$ and $e_2$ be the two Clifford bases. They satisfy the following properties:

$$e_1^2=-1, \quad e_2^2=-1, \quad e_1e_2=-e_2e_1, \tag{54}$$

$$\overline{e_1}=-e_1, \quad \overline{e_2}=-e_2, \tag{55}$$

where $\overline{s}$ is the conjugate of $s$. We regard points (vectors) $\xi=(x,y,z)\in R^3$ and their corresponding Clifford 1-vectors $\xi=x+ye_1+ze_2$ as equivalent. The same notation $\xi$ can either be a point or its corresponding 1-vector in different contexts: for example, for vectors $\xi$ and $\eta$, the multiplication $\xi\eta$ is obtained through Clifford multiplication by regarding $\xi$ and $\eta$ as their Clifford 1-vector counterparts; for Clifford 1-vectors $\xi$, $\eta$ and $\zeta$, $\xi(\eta\times\zeta)$ is obtained by first regarding $\eta$ and $\zeta$ as vectors and calculating the cross product $\eta\times\zeta$, then rewriting $\eta\times\zeta$ as its corresponding Clifford 1-vector and calculating the Clifford multiplication between $\xi$ and $\eta\times\zeta$. We also use the notation $\xi_\alpha=x_\alpha+y_\alpha e_1+z_\alpha e_2$.

Clifford algebra shares several important properties of complex variables. For example, we can show using (54)–(55) that

$$\xi\overline{\xi}=(x+ye_1+ze_2)(x-ye_1-ze_2)=x^2+y^2+z^2=|\xi|^2, \tag{56}$$

and

$$\frac{1}{\xi}=\frac{\overline{\xi}}{|\xi|^2}, \quad \frac{1}{\overline{\xi}}=\frac{\xi}{|\xi|^2}. \tag{57}$$

Now regarding $\mathbf{z}$ as Clifford 1-vector, we can rewrite the evolution equation (52) as follows:

$$\frac{\partial \mathbf{z}(\alpha,t)}{\partial t}=-\frac{1}{2\overline{\mathbf{z}}_{\alpha_1}(\alpha,t)}+V_1(\alpha,t), \tag{58}$$

where $V_1$ is still defined by (45) with $\mathbf{z}$ as a Clifford 1-vector.

To derive an equation for $\overline{\mathbf{z}}$, we take the conjugate of the both sides of (53). We get

$$\frac{\partial \overline{\mathbf{z}}(\alpha,t)}{\partial t}=\frac{1}{2\mathbf{z}_{\alpha_1}(\alpha,t)}+\overline{V_2}(\alpha,t), \tag{59}$$

where $\overline{V_2}$ is defined as

$$\overline{V_2}(\alpha,t)=\lim_{\substack{(x-ye_1-ze_2)\to\overline{\mathbf{z}}(\alpha,t)\\ y<y(\alpha,t)}}\int |\nabla_\alpha \mu(\alpha')^T, \nabla_\alpha \overline{\mathbf{z}}(\alpha',t)^T| \times \nabla_{\overline{z}'}G(\overline{\mathbf{z}}-\overline{\mathbf{z}}(\alpha',t))d\alpha'. \tag{60}$$

For the case we consider, $\mathbf{z}$ is a periodic perturbation over a flat surface, i.e. $\mathbf{z}=\alpha_1+\alpha_2e_1+\mathbf{s}$ with $\mathbf{s}=S_1+S_2e_1+S_3e_2$ being double periodic in $\alpha$. We can further rewrite the above equations in terms of $\mathbf{s}$. We get

$$\frac{\partial \mathbf{s}(\alpha,t)}{\partial t}=-\frac{1}{2(1+\overline{\mathbf{s}}_{\alpha_1})}+V_1(\alpha,t), \tag{61}$$

$$\frac{\partial \overline{\mathbf{s}}(\alpha,t)}{\partial t}=\frac{1}{2(1+\mathbf{s}_{\alpha_1})}+\overline{V_2}(\alpha,t). \tag{62}$$

Observe that the leading order terms on the right hand sides of (61)–(62) only involve derivatives in $\alpha_1$. This implies that $\alpha_1$ is the most unstable direction responsible for generating the Kelvin–Helmholtz instability. The $\alpha_2$ direction is in a stable direction. This observation suggests that we need only complexify the $\alpha_1$ variable and treat $\alpha_2$ as a real parameter which parametrizes the singularity curve in the extended complex $\alpha_1$ domain. To better illustrate the main idea, we will suppress the dependence of $\mathbf{s}$ on $\alpha_2$, and write $\mathbf{s}(\alpha_1,t)$. Following Caflisch and Orellana[6] and Cowley, Baker and Tanveer,[8] we extend $\mathbf{s}(\alpha_1,t)$ and $\overline{\mathbf{s}}$ to the upper half complex $\alpha_1$ domain. We say $\mathbf{s}(\alpha_1)$ is analytic if each component of $\mathbf{s}$ is analytic with respect to $\alpha_1$. In particular, if $\mathbf{s}(\alpha_1,t)$ has a convergent Taylor series expansion in a neighborhood of $\alpha_{10}$, then we say that $\mathbf{s}(\alpha_1,t)$ is analytic at $\alpha_{10}$.

To unify notations, we will denote the complex $\alpha_1$ variable as $\alpha_1=\text{Real}(\alpha_1)+\text{Im}(\alpha_1)e_1$, and regard $\alpha_1$ as a Clifford 1-vector. In particular, the analytic extension of the conjugate function $\overline{s}(\alpha_1,t)$ is defined by the following $*$ operator:

$$\mathbf{s}^*(\alpha_1,t)=\overline{\mathbf{s}(\overline{\alpha_1},t)}. \tag{63}$$

Now analytically extending Eqs. (61)–(62) to the upper half complex $\alpha_1$ domain, we obtain

$$\frac{\partial \mathbf{s}(\alpha_1,t)}{\partial t}=\frac{\mathbf{s}^*_{\alpha_1}}{2(1+\mathbf{s}^*_{\alpha_1})}+\left(V_1(\alpha_1,t)-\frac{1}{2}\right), \tag{64}$$

$$\frac{\partial \mathbf{s}^*(\alpha_1,t)}{\partial t} = -\frac{\mathbf{s}_{\alpha_1}}{2(1+\mathbf{s}_{\alpha_1})} + \left(\overline{V_2}(\alpha_1,t) + \frac{1}{2}\right), \tag{65}$$

at $t=0$.

Note that when we analytically extend $\mathbf{s}$ to the upper half complex $\alpha_1$ domain, the integrals in $V_1$ and $V_2$ are no longer singular. In fact, one can show that in the regions of the complex $\alpha_1$ domain where

$$\mathrm{Im}(\alpha_1) \gg 1 \quad \text{and} \quad \mathbf{s} = O(1), \tag{66}$$

we have

$$V_1(\alpha_1,t) = o(1) \quad \text{and} \quad V_2(\alpha_1,t) = o(1), \quad \text{as } \mathrm{Im}(\alpha_1) \to \infty. \tag{67}$$

This is easy to see over one period in the $\alpha'$ variable since

$$|\nabla_{\mathbf{z}'} G(\mathbf{z}-\mathbf{z}')| \leq \frac{C}{|\mathrm{Im}(\alpha_1)|^2 + |\mathrm{Re}(\alpha-\alpha')|^2}, \tag{68}$$

which tends to zero as $\mathrm{Im}(\alpha_1) \to \infty$. The contributions from other periodic images can be estimated using the Ewald summation formula.[18] Note that the integral in $V_1$ or $V_2$ involves the derivatives of $\mathbf{z}(\alpha',t)$. Since the derivatives $\mathbf{z}_{\alpha_i}$ $(i=1,2)$ are evaluated only at *real* $\alpha'$, the integrand remains small even at the points where the leading order local terms blow up, which corresponds to either $(1+\mathbf{s}_{\alpha_1})=0$ or $(1+\mathbf{s}^*_{\alpha_1})=0$.

The above local system is a generalization of the local system obtained by Cowley, Baker and Tanveer in Ref. 8 for 2-D vortex sheets. For each $\alpha_2$ fixed, we can apply the same analysis developed by Cowley, Baker and Tanveer[8] to show that $\mathbf{s}$ and $\mathbf{s}^*$ develop singularities of order 3/2 in the extended $\alpha_1$ domain at $t=0^+$. For the sake of completeness, we outline some of the key steps in the early time singularity analysis of Cowley, Baker and Tanveer.[8] There are two cases. In case one, there exists $\alpha_{10}$ such that $1+\mathbf{s}_{\alpha_1}(\alpha_{10})$ and $1+\mathbf{s}^*_{\alpha_1}(\alpha_{10})$ vanish simultaneously. In case two, there exists $\alpha_{10}$ such that only one of two quantities mentioned above vanishes at $\alpha_{10}$. We only demonstrate the second case in which we assume

$$1+\mathbf{s}_{\alpha_1}(\alpha_{10}) = 0,$$

but

$$1+\mathbf{s}^*_{\alpha_1}(\alpha_{10}) \neq 0.$$

As noted by Cowley, Baker and Tanveer,[8] one needs to introduce a rescaling near $\alpha_1=\alpha_{10}$. In order to determine the appropriate asymptotic structure, we expand the solution $\mathbf{s}$ and $\mathbf{s}^*$ first in time and then in space near $\alpha_1=\alpha_{10}$. Let $\zeta=\alpha_1-\alpha_{01}$. We have

$$\mathbf{s} = \mathbf{s}_{00} + \mathbf{s}_{01}\zeta + \frac{1}{2}\mathbf{s}_{02}\zeta^2 + \cdots + \left(\frac{\mathbf{s}^*_{01}}{2(1+\mathbf{s}^*_{01})} + K_{00}\right)t + \cdots, \tag{69}$$

$$\mathbf{s}^* = \mathbf{s}^*_{00} + \mathbf{s}^*_{01}\zeta + \frac{1}{2}\mathbf{s}^*_{02}\zeta^2 + \cdots + \left(\frac{-\mathbf{s}_{01}}{2\mathbf{s}_{02}\zeta} + \cdots\right)t + \cdots, \tag{70}$$

where

$$s_{0n} = \frac{\partial^n s}{\partial \alpha_1^n}(\alpha_{10},0), \quad s^*_{0n} = \frac{\partial^n s^*}{\partial \alpha_1^n}(\alpha_{10},0),$$

and

$$K_{00} = V_1(\alpha_{10},0) - \frac{1}{2}.$$

The nonuniformity arises from the leading order coefficient of the $O(t)$ term in (70). The leading coefficient of the $O(t)$ term in (70) plays a determining role in the asymptotic structure. This indicates that the key terms are those including $\mathbf{s}^*_{01}$ and $\mathbf{s}_{02}$. These terms are comparable in (70) when $\zeta = O(t^{1/2})$. This consideration suggests that the asymptotic scaling for small $\zeta$ when $t \ll 1$ is

$$\zeta = \eta\omega t^{1/2}, \quad \text{where} \quad \omega = \left|\frac{2}{\mathbf{s}_{02}(1+\mathbf{s}^*_{01})}\right|^{1/2}. \tag{71}$$

Using this asymptotic scaling, we expand $\mathbf{s}$ and $\mathbf{s}^*$ as follows:

$$\mathbf{s} = \mathbf{s}_{00} + \mathbf{s}_{01}\eta\omega t^{1/2} + \left(\frac{1}{2} + K_{00} + \frac{1}{1+\mathbf{s}^*_{01}}A(\eta)\right)t + \cdots, \tag{72}$$

$$\mathbf{s}^* = \mathbf{s}^*_{00} + ((1+\mathbf{s}^*_{01})B(\eta) - \eta)\omega t^{1/2} + \cdots. \tag{73}$$

The functions $A(\eta)$ and $B(\eta)$ will be determined from the evolution equations of $\mathbf{s}$ and $\mathbf{s}^*$. Using a careful analysis which is supplemented by numerical study, Cowley, Baker and Tanveer[8] showed that $A(\eta)$ and $B(\eta)$ have a branch point singularity of order 3/2 at a certain point $\eta_0$. In particular, $A(\eta)$ and $B(\eta)$ have the expansions

$$A(\eta) = A_0 + A_1(\eta-\eta_0) + A_p(\eta-\eta_0)^p + \cdots, \tag{74}$$

$$B(\eta) = B_0 + B_1(\eta-\eta_0) + B_p(\eta-\eta_0)^p + \cdots, \tag{75}$$

in the neighborhood of $\eta_0$ with $A_1B_1 \neq 0$, $p=\frac{3}{2}$. Thus we conclude that $\mathbf{s}$ and $\mathbf{s}^*$ form a singularity of order 3/2 spontaneously at $t=0^+$.

In the above derivation, the complex conjugate of (53) is analytically continued into the upper half complex $\alpha_1$-plane, using conjugate variable $\mathbf{s}^*$. This is equivalent to analytically continuing the equation into the lower half of the complex $\alpha_1$-plane using $\mathbf{s}$ because of the definition of $\mathbf{s}^*(\alpha_1,t) = \overline{\mathbf{s}(\overline{\alpha_1},t)}$. Therefore, the directions towards which the analytical continuations take place are, in fact, opposite for (64) and (65). As a result, it provides the coupling from $\mathbf{s}$ on the upper half complex $\alpha_1$-domain to $\mathbf{s}$ on the lower half complex $\alpha_1$-domain by introducing $\mathbf{s}^*$. It is worth noting that it is the coupling that generates the Kelvin–Helmholtz instability.

### B. Existence of the orthogonal coordinates

In the analysis presented in the previous subsection, we have assumed that $(\alpha_1,\alpha_2)$ satisfies (49) and (50). Now we show that for a reasonably large class of $\mu$, we can always find another coordinate system $(\beta_1,\beta_2)$ such that Eqs. (49) and (50) are satisfied, i.e.,

$$\mathbf{z}_{\beta_1}\cdot\mathbf{z}_{\beta_2}=0,\quad \frac{\partial\mu}{\partial\beta_1}=1,\quad \frac{\partial\mu}{\partial\beta_2}=0.$$

To satisfy $\partial\mu/\partial\beta_1=1$, we clearly should take $\beta_1=\mu(\alpha)$. With this choice of $\beta_1$, we can show that

$$\frac{\partial\mu}{\partial\beta_2}=\mu_{\alpha_1}\alpha_{1_{\beta_2}}+\mu_{\alpha_2}\alpha_{2_{\beta_2}}=\frac{1}{\Delta}(-\mu_{\alpha_1}\beta_{1_{\alpha_2}}+\mu_{\alpha_2}\beta_{1_{\alpha_1}})=0, \tag{76}$$

since $\beta_1=\mu$. Here we have used the relationship

$$\frac{\partial(\alpha_1,\alpha_2)}{\partial(\beta_1,\beta_2)}=\frac{1}{\Delta}\begin{pmatrix}\beta_{2_{\alpha_2}} & -\beta_{1_{\alpha_2}}\\ -\beta_{2_{\alpha_1}} & \beta_{1_{\alpha_1}}\end{pmatrix}. \tag{77}$$

We have assumed that the Jacobian $\Delta$ of the transform $\beta(\alpha)$ is nonzero, i.e.,

$$\Delta\equiv\beta_{1_{\alpha_1}}\beta_{2_{\alpha_2}}-\beta_{1_{\alpha_2}}\beta_{2_{\alpha_1}}\neq 0.$$

The next step is to choose $\beta_2$ to satisfy the orthogonality condition, $\mathbf{z}_{\beta_1}\cdot\mathbf{z}_{\beta_2}=0$, i.e.,

$$\left(z_{\alpha_1}\frac{\partial\alpha_1}{\partial\beta_1}+z_{\alpha_2}\frac{\partial\alpha_2}{\partial\beta_1}\right)\cdot\left(z_{\alpha_1}\frac{\partial\alpha_1}{\partial\beta_2}+z_{\alpha_2}\frac{\partial\alpha_2}{\partial\beta_2}\right)=0. \tag{78}$$

Define $\lambda_1(\alpha_1,\alpha_2)$ and $\lambda_2(\alpha_1,\alpha_2)$ as

$$\lambda_1(\alpha_1,\alpha_2)=\frac{z_{\alpha_1}\cdot z_{\alpha_1}}{z_{\alpha_2}\cdot z_{\alpha_2}}, \tag{79}$$

$$\lambda_2(\alpha_1,\alpha_2)=\frac{z_{\alpha_1}\cdot z_{\alpha_2}}{z_{\alpha_2}\cdot z_{\alpha_2}}. \tag{80}$$

Note that in the case that the interface is a small perturbation of a flat plane, $\lambda_i$ is a small perturbation of a constant. By substituting (79)–(80) into Eq. (78), we get

$$\lambda_1\frac{\partial\alpha_1}{\partial\beta_1}\frac{\partial\alpha_1}{\partial\beta_2}+\frac{\partial\alpha_2}{\partial\beta_1}\frac{\partial\alpha_2}{\partial\beta_2}+\lambda_2\left(\frac{\partial\alpha_1}{\partial\beta_1}\frac{\partial\alpha_2}{\partial\beta_2}+\frac{\partial\alpha_2}{\partial\beta_1}\frac{\partial\alpha_1}{\partial\beta_2}\right)=0.$$

By applying (77), we obtain

$$-\lambda_1\frac{\partial\beta_2}{\partial\alpha_2}\frac{\partial\beta_1}{\partial\alpha_2}-\frac{\partial\beta_2}{\partial\alpha_1}\frac{\partial\beta_1}{\partial\alpha_1}+\lambda_2\left(\frac{\partial\beta_2}{\partial\alpha_2}\frac{\partial\beta_1}{\partial\alpha_1}+\frac{\partial\beta_2}{\partial\alpha_1}\frac{\partial\beta_1}{\partial\alpha_2}\right)=0.$$

Furthermore, substituting $\beta_1=\mu$ to the above equation leads to

$$\left(\lambda_1\frac{\partial\mu}{\partial\alpha_2}-\lambda_2\frac{\partial\mu}{\partial\alpha_1}\right)\frac{\partial\beta_2}{\partial\alpha_2}+\left(\frac{\partial\mu}{\partial\alpha_1}-\lambda_2\frac{\partial\mu}{\partial\alpha_2}\right)\frac{\partial\beta_2}{\partial\alpha_1}=0. \tag{81}$$

Note that the equation for $\beta_2$ is a first order linear hyperbolic equation. Therefore it is well-posed. Further, if we assume that the interface is a small perturbation of a flat plane, and $\gamma_i$ are near constants, then we can solve for $\beta_2$ explicitly by a line integral as in (40) to the leading order. In this case, we can show that the Jacobian $\Delta=\gamma_1^2+\gamma_2^2+O(\epsilon)>0$. In general, we can show that $\Delta$ will always be a small perturbation of some nonzero constant. This proves the existence of the orthogonal coordinates $(\beta_1,\beta_2)$ satisfying (49) and (50).

*Remark:* The above construction of the orthogonal coordinates can be applied to the vortex sheet solution at any given time. Note that we always have $\beta_1=\mu(\alpha)$. If $\alpha$ is the Lagrangian variable, then $\mu(\alpha)$ is time independent. On the other hand, $\beta_2=\beta_2(\alpha)$ is time dependent. Thus, when we view the solution in the original coordinate $(\alpha_1,\alpha_2)$, the vortex sheet solution can have singularity in both $\alpha_1$ and $\alpha_2$ through the coordinate mapping $\alpha=\alpha(\beta,t)$ dynamically.

### C. Motion of the singularities

In the previous subsection, we have shown how to derive a local approximate system for 3-D vortex sheets and how to use the corresponding 2-D analysis to show that singularities of order 3/2 develop spontaneously at $t=0+$ in the complex $\alpha_1$ domain around the positions where $(1+\mathbf{s}_{\alpha_1})=0$ and/or $(1+\mathbf{s}^*_{\alpha_1})=0$. This implies that the singularities develop simultaneously along one or several one-dimensional curves parametrized by $\beta_2$, i.e., $\beta_1(\beta_2,t)$. Once the complex singularities of order 3/2 are formed initially, they generically do not change type in time. As time increases, each point on these one-dimensional curves moves around in the complex $\beta_1$ domain. The physical singularity time is the first time when these curves hit the real $\beta_1$ axis.

In this subsection, we show that at any time $t$ before the singularity time, the one-dimensional singularity curve in the complex $\beta_1$ domain, denoted as $\xi_s(\beta_2,t)$, is always an analytical function of $\beta_2$. Due to the analyticity of $\xi_s(\beta_2,t)$ as a function of $\beta_2$, the curve $\xi_s(\beta_2,t)$ cannot intersect with the real $(\beta_1,\beta_2)$ plane in a segment, for if this were the case it would imply that the entire curve has a zero imaginary part by analytic continuation. Therefore, its intersection with the real $(\beta_1,\beta_2)$ plane contains either isolated points, or the entire $\xi_s(\beta_2,t)$ curve. In the latter case, the vortex sheet surface becomes singular along an entire one-dimensional curve at the singularity time.

At time $t=0+$, from the results of the previous section, $\xi_s(\beta_2,0)$ is defined implicitly by $1+\mathbf{s}(\xi_s(\beta_2,0),\beta_2,0)=0$ or $1+\mathbf{s}^*(\xi_s(\beta_2,0),\beta_2,0)=0$. Since the initial condition is assumed to be analytic in both $\beta_1$ and $\beta_2$, we conclude that $\xi_s(\beta_2,0)$ is an analytic function of $\beta_2$.

To derive an evolution equation for $\xi_s(\beta_2,t)$, we follow the analysis in Ref. 8. Close to the singularity we seek an asymptotic expansion of the form

$$\mathbf{s}=S_0(\beta_2,t)+S_1(\beta_2,t)\,\eta+S_p(\beta_2,t)\,\eta^p+\cdots, \tag{82}$$

$$\mathbf{s}^*=S_0^*(\beta_2,t)+S_1^*(\beta_2,t)\,\eta+S_p^*(\beta_2,t)\,\eta^p+\cdots, \tag{83}$$

where we now define $\eta=\xi-\xi_s(\beta_2,t)$. Substituting (82)–(83) into (64)–(65) with the dynamically reparametrized coordinate $(\beta_1,\beta_2)$, and equating like powers of $\eta$, we find that (82)–(83) is an acceptable local solution if the following compatibility conditions are satisfied:

$$\begin{aligned}\dot S_0-\dot\xi_s S_1&=\frac{S_1^*}{2(1+S_1^*)}+K(\xi_s,t),\\ \dot S_0^*-\dot\xi_s S_1^*&=-\frac{S_1}{2(1+S_1)}+J(\xi_s,t),\end{aligned} \tag{84}$$

$$\dot{\xi}_s^2 = -\left(\frac{1}{2(1+S_1)(1+S_1^*)}\right)^2, \quad S_p = (2(1+S_1)^2 S_p^*)\dot{\xi}_s, \tag{85}$$

where an overdot denotes differentiation with respect to time. Note that the dynamical reparametrization introduces a tangential velocity field to the right-hand sides of (64)–(65) in the form of

$$\mathbf{z}_{\beta_1}\frac{\partial \beta_1}{\partial t} + \mathbf{z}_{\beta_2}\frac{\partial \beta_2}{\partial t}.$$

This corresponds to choosing $T^1 = \partial\beta_1/\partial t\,|\mathbf{z}_{\beta_1}|$ and $T^1 = \partial\beta_2/\partial t\,|\mathbf{z}_{\beta_2}|$ in (10)–(11). Note that in the original Lagrangian variable $\alpha$, the dipole strength $\mu(\alpha)$ is time independent. Thus we have $\partial\beta_1/\partial t = 0$ since $\beta_1 = \mu(\alpha)$. One can derive an equation for $\partial\beta_2/\partial t$ by differentiating Eq. (81) in time and using the evolution equation. From Eq. (81), we can conclude that $\partial\beta_2/\partial t$ has the same order of regularity as $\mathbf{z}_{\beta_i}$ $(i=1,2)$. Thus the $\partial\beta_2/\partial t\,(\xi_s,t)$ is well defined. Taking into account this added tangential velocity field, which we denote as $V_T = \mathbf{z}_{\beta_2}\partial\beta_2/\partial t$, we have $K(\xi_s,t) = (V_1+V_T)\times(\xi_s,t) - \frac{1}{2}$, and $J(\xi_s,t) = \overline{(V_2+V_T)}(\xi_s,t) + \frac{1}{2}$. Since $S_0$, $S_1$ and $S_0^*$, $S_1^*$ are analytic in $\beta_2$, we conclude that $\xi_s$ is analytic in $\beta_2$. As a result, we show that when physical singularities appear, they appear either at some isolated points, or along the entire one-dimensional curve in the real $(\beta_1,\beta_2)$ plane. It is not possible for the interface to develop finite time singularities along a segment of a one-dimensional curve.[27] This result will be confirmed by our numerical results.

### D. The local form of the curvature singularity

Our arguments in the previous subsection show that singularities of order 3/2 develop at the complex $\alpha_1$ domain where $|\mathrm{Im}(\alpha_1)| \gg 1$ at $t = 0^+$. As time increases, the singularities propagate in the extended $\alpha_1$ complex domain. The first time at which their trajectories intersect the real $\alpha_1$ axis gives the time that a physical singularity appears. In this subsection, we study the local form of the interface shape in the neighborhood of the physical singularity.

Without loss of generality, we assume that the singularity forms at $t=0$ and $(\alpha_1,\alpha_2)=(0,0)$, and that the surface is moving with a velocity of $\dot{\mathbf{z}}$ at that point. We also assume that at the time of singularity formation, the surface is locally flat in the neighborhood of the singularity, with $\mathbf{z} \sim \mathbf{z}_0(\alpha_1,\alpha_2)$, where $\mathbf{z}_0$ is a plane.

Motivated by our leading order analysis near equilibrium, we introduce a *time independent* change of variables from $\alpha$ to $\beta$ given by (39)–(40). To simplify our presentation, we may assume that such a change of variables has been made at $t=0$. We will still denote $\beta$ as $\alpha$. It is easy to check that in this new coordinate, we have

$$\frac{\partial \mu}{\partial \alpha_1} = 1, \quad \frac{\partial \mu}{\partial \alpha_2} = 0. \tag{86}$$

We seek an asymptotic expansion of the solution of the three-dimensional vortex sheet equation (9). Following the idea of Cowley, Baker and Tanveer,[8] we separate the integral on the right-hand side of (8) into two regions: a local region where $|\alpha'| = O(t)$ and an outer region covering the rest of the sheet,

$$\frac{\partial \mathbf{z}}{\partial t}(\alpha,t) = \left(\int_{|\alpha'|>\delta} + \int_{|\alpha'|\le\delta}\right) |\nabla_\alpha \mu(\alpha')^T, \nabla_\alpha \mathbf{z}(\alpha',t)^T| \times \nabla_{\mathbf{z}'} G(\mathbf{z}(\alpha,t) - \mathbf{z}(\alpha',t))\, d\alpha'. \tag{87}$$

In order to determine the local shape of the vortex sheet near the singularity, it is not necessary to consider the first integral in detail, other than to note that in the Taylor expansion of $\mathbf{z}(\alpha,t)$ in powers of t, the first two terms of the asymptotic expansion can be assumed to be $O(t^0)$ and $O(t^1)$, as in Cowley, Baker and Tanveer.[8] This means that the leading order contribution from the first integral is of order $O(t^0)$. It also suggests that the leading order correction terms from the first integral is smaller than that of the second integral, as we will show later. Therefore, the shape of the vortex sheet in the neighborhood of the singularity is essentially determined by the second integral. In order to approximate the singularity, it is convenient to write $\mathbf{z}$ in the form of components on the two tangential and one normal directions:

$$\mathbf{z} = \dot{\mathbf{z}}_0 t + \begin{pmatrix} \mathbf{z}_0^{\mathbf{t}_1} \\ \mathbf{z}_0^{\mathbf{t}_2} \\ \mathbf{z}_0^{\mathbf{n}} \end{pmatrix} + \begin{pmatrix} P_1(\alpha,t) \\ P_2(\alpha,t) \\ P_3(\alpha,t) \end{pmatrix}, \tag{88}$$

where

$$\mathbf{z}_0^{\mathbf{t}_1} = \mathbf{z}_0 \cdot \mathbf{t}_1, \quad \mathbf{z}_0^{\mathbf{t}_2} = \mathbf{z}_0 \cdot \mathbf{t}_2, \quad \mathbf{z}_0^{\mathbf{n}} = \mathbf{z}_0 \cdot \mathbf{n},$$

and

$$\mathbf{t}_1 = \frac{\mathbf{z}_{0_{\alpha_1}}}{|\mathbf{z}_{0_{\alpha_1}}|}, \quad \mathbf{t}_2 = \frac{\mathbf{z}_{0_{\alpha_2}}}{|\mathbf{z}_{0_{\alpha_2}}|},$$

$$\mathbf{n} = \frac{\mathbf{z}_{0_{\alpha_1}} \times \mathbf{z}_{0_{\alpha_2}}}{|\mathbf{z}_{0_{\alpha_1}} \times \mathbf{z}_{0_{\alpha_2}}|},$$

where $P_1$, $P_2$ and $P_3$ are small perturbations of the interface from the tangent plane in the $\mathbf{t}_1$, $\mathbf{t}_2$ and $\mathbf{n}$ directions, respectively.

We substitute (88) into the second integral of the three-dimensional vortex sheet equation and seek asymptotic expansions of $P_i$'s. We follow the analysis by Hou and Zhang[13] in which they studied the growth rate for the linearized motion about an arbitrary smooth solution to the three-dimensional vortex sheet equation. In our case, we can use their result directly because a flat plane is an equilibrium state of Eq. (8), and therefore, the leading order terms extracted from the asymptotic expansion coincide with the leading order terms in the linearized equation.

Motivated by the leading order analysis near equilibrium in Sec. II B and the analysis in Hou and Zhang,[13] we introduce a change of variables from $(P_1,P_2)$ to $(\phi_1,\phi_2)$ as follows:

$$\phi_1 = (\sigma_2)^{-1}\tilde{H}_2 P_1 - (\sigma_1)^{-1}\tilde{H}_1 P_2, \tag{89}$$

$$\phi_2=(\sigma_1)^{-1}\tilde{H}_1P_1+(\sigma_2)^{-1}\tilde{H}_2P_2, \tag{90}$$

where $\tilde{H}_1$ and $\tilde{H}_2$ are the Riesz transforms defined on the interface,

$$(\overline{H_l}f)(\alpha) = \frac{1}{2\pi}\int \frac{(\alpha_l-\alpha_l')f(\alpha')}{|\mathbf{z}_{0_{\alpha_1}}(\alpha)(\alpha_1-\alpha_1')+\mathbf{z}_{0_{\alpha_2}}(\alpha)(\alpha_2-\alpha_2')|^3}d\alpha', \tag{91}$$

and $\sigma_l^{-1}=|\mathbf{z}_{0_{\alpha_l}}|$ with $l=1,2$. Using the property (86) of our coordinate, we can greatly simplify the leading order system derived by Hou and Zhang.[13] By using the properties of the Riesz transforms [see Lemma 4.4 and Eqs. (41)–(42) in Hou and Zhang[13]], we obtain the following leading order approximation to the 3-D vortex sheet equation:

$$\frac{\partial\phi_1}{\partial t}=E_1(\phi_1,\phi_2,P_3), \tag{92}$$

$$\frac{\partial\phi_2}{\partial t}=\frac{1}{2}\sigma_1^3\sigma_2\frac{\partial P_3}{\partial\alpha_1}+E_2(\phi_1,\phi_2,P_3), \tag{93}$$

$$\frac{\partial P_3}{\partial t}=-\frac{1}{2}\sigma_1^5\sigma_2^3\frac{\partial\phi_2}{\partial\alpha_1}+\frac{1}{2}\sigma_1^4\sigma_2^4\frac{\partial\phi_1}{\partial\alpha_2}+E_3(\phi_1,\phi_2,P_3), \tag{94}$$

where $E_1$, $E_2$ and $E_3$ are the general representations of terms that are either smaller or smoother than the leading order terms, provided that the perturbations are of small amplitude. While the Hou and Zhang analysis is for smooth solutions, their result can also be generalized to interfaces that develop singularities of order 3/2. Moreover, the assumption of an orthogonal coordinate in Hou and Zhang[13] is not necessary. It can be removed using the analysis of a related paper by Hou and Zhang[22] [see (67) on p. 15 of Hou and Zhang[22]]. The additional terms due to the nonorthogonal coordinate [see Eqs. (74)–(75) on p. 17 of Hou and Zhang[22]] contribute only to the lower order terms since we assume the interface is a small perturbation near the equilibrium. A variant of this result has been proved by Caflisch and Semmes[12] for 2-D vortex sheets. An estimate similar to Caflisch and Semmes can also be derived for 3-D surfaces using Clifford algebra representation. To illustrate, we first consider the 2-D case. A typical term in $E_i$ consists of

$$\frac{1}{\pi}\int\left(\frac{1}{\mathbf{z}(\alpha)-\mathbf{z}(\alpha')}-\frac{1}{\mathbf{z}_\alpha(\alpha')(\alpha-\alpha')}\right)d\alpha'.$$

Let $\mathbf{z}(\alpha)=\alpha+\mathbf{s}(\alpha)$, and assume that $\mathbf{s}$ is of a small amplitude. Thus we have $\mathbf{z}_\alpha=1+\mathbf{s}_\alpha$. By expanding $1/(1+\mathbf{s}_\alpha)$ in Taylor series, we get

$$\begin{aligned}\frac{1}{\pi}\int\frac{1}{\mathbf{z}_\alpha(\alpha')(\alpha-\alpha')}d\alpha' &= \frac{1}{\pi}\sum_{k=0}^{\infty}(-1)^k\int\frac{\mathbf{s}_\alpha(\alpha')^k}{(\alpha-\alpha')}d\alpha' \\ &= \sum_{k=0}^{\infty}(-1)^kH(\mathbf{s}_\alpha^k),\end{aligned} \tag{95}$$

where $H$ is the Hilbert transform, $H(f)(\alpha)=1/\pi\int[f(\alpha')/(\alpha-\alpha')]\,d\alpha'$. Similarly, we have

$$\frac{1}{\pi}\int\frac{1}{\mathbf{z}(\alpha)-\mathbf{z}(\alpha')}d\alpha' = \frac{1}{\pi}\sum_{k=0}^{\infty}(-1)^k\int\frac{(\mathbf{s}(\alpha)-\mathbf{s}(\alpha'))^k}{(\alpha-\alpha')^{k+1}}d\alpha'. \tag{96}$$

Comparing Eq. (96) with Eq. (95) term by term, we find that the zeroth order terms in both equations vanish. For the leading order linear term from Eq. (96), integration by parts implies that

$$\frac{1}{\pi}\int\frac{(\mathbf{s}(\alpha)-\mathbf{s}(\alpha'))}{(\alpha-\alpha')^2}d\alpha'=H(\mathbf{s}_\alpha),$$

which cancels exactly the linear term from Eq. (95). For the quadratic term from Eq. (96), we have after performing integration by parts twice,

$$\frac{1}{\pi}\int\frac{(\mathbf{s}(\alpha)-\mathbf{s}(\alpha'))^2}{(\alpha-\alpha')^3}d\alpha' = H(\mathbf{s}_\alpha^2)-\frac{1}{\pi}\int\frac{(\mathbf{s}(\alpha)-\mathbf{s}(\alpha'))}{(\alpha-\alpha')}\mathbf{s}_{\alpha'\alpha'}(\alpha')d\alpha',$$

which cancels the corresponding quadratic term in Eq. (95) with an error term of the form

$$\frac{1}{\pi}\int\frac{\mathbf{s}(\alpha)-\mathbf{s}(\alpha')}{(\alpha-\alpha')}\mathbf{s}_{\alpha'\alpha'}(\alpha')d\alpha'. \tag{97}$$

If $\mathbf{s}(\alpha)$ has a singularity of order 3/2, in other words, $\mathbf{s}(\alpha)$ has 3/2 order regularity (in $C^{3/2}$), then the kernel $(\mathbf{s}(\alpha)-\mathbf{s}(\alpha'))/(\alpha-\alpha')$ is a smoothing kernel of order 3/2. This means that we can gain 3/2 order regularity to the singular integrand $\mathbf{s}_{\alpha'\alpha'}$ in Eq. (97). Therefore, we argue that the error term given by Eq. (97) is a half order smoother than the leading order term, which is of order $\mathbf{s}_\alpha$. Because of the nonlinearity, the error term is also smaller in amplitude. This argument can continue to higher order terms. For example, for the third order terms, the error functions have the following forms:

$$\frac{1}{\pi}\int\left(\frac{\mathbf{s}(\alpha)-\mathbf{s}(\alpha')}{\alpha-\alpha'}\right)(\mathbf{s}_{\alpha'}^2)_{\alpha'}(\alpha')d\alpha',$$

or

$$\frac{1}{\pi}\int\left(\frac{\mathbf{s}(\alpha)-\mathbf{s}(\alpha')}{\alpha-\alpha'}\right)^2\mathbf{s}_{\alpha'\alpha'}(\alpha')d\alpha'.$$

In either case, we have a smoothing kernel of order 3/2. Thus the same argument used for the quadratic terms applies.

The above argument can be generalized to the 3-D case by using the Taylor expansion in terms of the small perturbations $(S_1, S_2, S_3)$. Instead of dealing with the Hilbert transform as in the 2-D case, we now have to deal with the Riesz transform. Since the derivations are quite technical, we would not present them here. Our numerical experiments have also confirmed that the error terms are generically one half order smoother than the leading order terms for functions with singularity of order 3/2.

Next we study the self-similar singularity solution of the leading order approximate system. Following the idea by Cowley, Baker and Tanveer,[8] we introduce a rescaling by

$$\alpha_1 = (-t)\chi, \tag{98}$$

and seek similarity solutions of the form

$$\phi_1 = (-t)^q F_1(\alpha_2, \chi) + \cdots, \tag{99}$$

$$\phi_2 = (-t)^q F_2(\alpha_2, \chi) + \cdots, \tag{100}$$

$$P_3 = (-t)^q F_3(\alpha_2, \chi) + \cdots, \tag{101}$$

where $q > 1$ in order to be consistent with the assumption of the sheet being locally flat in the neighborhood of singularity. Since we have shown that branch point singularities in the $\alpha_1$ variable develop at $t = 0+$, we anticipate that $F_i \sim F_{i_\pm} |\chi|^q$ as $\chi \to \infty$, in order to match with the "outer" region where $\alpha_1 = O(1)$. For the initial conditions analyzed in the previous subsection, we have $q = 3/2$.

With the rescaling of (98), we substitute (99), (100) and (101) into (92), (93) and (94) and extract the $O((-t)^{-q+1})$ terms. It leads to

$$\chi F_{1_\chi} - qF_1 = 0, \tag{102}$$

$$\chi F_{2_\chi} - qF_2 = \frac{1}{2}\sigma_1^3 \sigma_2 F_{3_\chi}, \tag{103}$$

$$\chi F_{3_\chi} - qF_2 = -\frac{1}{2}\sigma_1^5 \sigma_2^3 F_{2_\chi} + \frac{(-t)}{2}\sigma_1^4 \sigma_2^4 F_{1_{\alpha_2}}. \tag{104}$$

Note that (102) has a zero forcing term. This suggests that there is no $q$th order singularity in the $\phi_1$ term. We conclude that $F_1 = 0$. Moreover, substituting this result into (103) and (104) leads to

$$\chi F_{2_\chi} - qF_2 = \frac{1}{2}\sigma_1^3 \sigma_2 F_{3_\chi}, \tag{105}$$

$$\chi F_{3_\chi} - qF_2 = -\frac{1}{2}\sigma_1^5 \sigma_2^3 F_{2_\chi}. \tag{106}$$

Since $\sigma_1 = 1 + O(\epsilon)$ and $\sigma_2 = 1 + O(\epsilon)$ are nearly constants in the neighborhood of the singularity, without loss of generality, we may assume that $\sigma_1 = 1$ and $\sigma_2 = 1$ to the leading order. Note that in Eqs. (105) and (106), $\alpha_2$ can be considered as a parameter, which shows that the essential direction in which singularities form is the $\alpha_1$ direction.

To solve (105) and (106), we substitute the leading order approximation $\sigma_1 = \sigma_2 = 1$ to Eqs. (105)–(106). Moreover, we define

$$F = F_2 + iF_3, \tag{107}$$

so that we can combine the system and obtain

$$\chi F' - qF = -\frac{1}{2} iF'. \tag{108}$$

By solving $F$ from (108), we obtain

$$F = C\left(\chi + \frac{1}{2} i\right)^q = C 2^{-q} (4\chi^2 + 1)^{q/2} \exp(iq \arctan((2\chi)^{-1})), \tag{109}$$

to the leading order, where $C$ is a function of $\alpha_2$ only.

The above analysis gives a leading order approximation of the possible singularity structure at the physical singularity time. However, it does not provide a mechanism to determine the exponent, $q$. The selection mechanism of the singularity type, i.e., the exponent $q$, is due to the strong nonlinear dynamic interaction at $t = 0+$. As we have shown in Sec. III A that the generic type is $q = 3/2$. Once the initial complex singularity is formed, it propagates along some analytic trajectory as we demonstrate in Sec. III C. Moreover, its type will not change dynamically.

An important consequence of the above analysis is that by projecting $(\mathbf{z}^{t_1}, \mathbf{z}^{t_2}, \mathbf{z}^{n})$ into $(\phi_1, \phi_2, \mathbf{z}^{n})$, we found that the curvature singularity does not appear on the $\phi_1$ function to the leading order at the singularity time. The curvature singularity of order 3/2 can be observed in the other two variables, $\phi_2$ and $\mathbf{z}^{n}$. This special feature will be confirmed later by our numerical study.

### E. A remark on the Brady and Pullin result

Before ending this section, we would like to demonstrate that our result is consistent with that of Brady and Pullin.[10] In a recent paper by Brady and Pullin,[10] they studied a three-dimensional vortex sheet with cylindrical shape and strength distribution at the same time. In particular, they assumed that, initially, the interface has a normal mode disturbance in the $z$ component of the form

$$h(x, y) = A \exp[i(mx + ny)], \tag{110}$$

with uniform velocity jump $U$ in the $x$-direction. By rotating from $(x, y, z)$ axes to $(x', y', z')$ axes with

$$kx' = mx + ny, \quad ky' = -nx + my, \quad z' = z, \tag{111}$$

where $k^2 = m^2 + n^2$, they showed that the singularity evolution in this special case is equivalent to that of a two-dimensional vortex sheet in $x' - z'$ variables with velocity jump of $Um/k$ along the $x'$ direction.

To apply our analysis to this special case, we take $x = \alpha_1$ and $y = \alpha_2$ at the initial time to fit the initial coordinates taken by Brady and Pullin.[10] Under this choice of coordinates, the transformations (89) and (90) applied to the normal mode is equivalent to a rotation of the axes. This is because the Fourier representations of the Riesz transforms are

$$\widehat{H_k}(\xi_1, \xi_2) = \frac{-i\xi_k}{(\xi_1^2 + \xi_2^2)^{1/2}}, \tag{112}$$

where $k=1,2$ and $(\xi_1,\xi_2)$ are the Fourier mode. Since the normal mode functions only have one Fourier mode, applying the Riesz transforms is equivalent to multiplying a constant factor to such functions. Specifically, the transformations (89) and (90) applied to normal mode initial condition (110) is equivalent to the axis rotation of (111). In this particular case, $\phi_1$ defined by (89) turns out to be zero, as has been proved by Brady and Pullin.[10] The strength of the singularity is proportional to the projection of the jump in the tangential velocity (in the $x$-direction) to the $x'$-direction. In particular, when we take $m=0$, which means that the direction along which the wave propagates is orthogonal to the $x$-direction, the singularity disappears. This shows that our result is consistent with the result of Brady and Pullin when we apply our analysis to their initial data.

## IV. A 3-D VORTEX SHEET MODEL EQUATION

All results in the previous section are based on formal asymptotic analysis. We need to perform a careful numerical study to confirm our analytical results. However, direct simulations of the three-dimensional vortex sheet equation are very expensive. The complexity in every time step is $O(N^4)$ by direct summation of the dipole representation, where $N$ is the number of particles used to discretize the surface in each dimension. Moreover, for initial conditions which are double periodic perturbations to the flat surface, one has to sum the contributions from all the periodic images. This adds substantially to the overall computational cost. It becomes prohibitively expensive even with $N$ at the level of $O(100)$. The fast multipole methods developed by Greengard and Rokhlin,[14] Berman and Greengard[15] can be used in principle to reduce the operating account to $cN^2$. However, the constant $c$ could be quite large in practice.

To alleviate the numerical difficulty mentioned above, we introduce a model equation for the three-dimensional vortex sheet problem. Our model equation has two important properties. First, it captures the leading order behavior of the singular solution for 3-D vortex sheets. In fact, we will show that our model equation forms the same tangential velocity jump condition as that of the full equation. Therefore, by applying the same analysis developed for the full equation, we can show that our model equation captures the singularity type of the full equation. We also show that the local singularity structure of our model equation has the same form as that of the full equation near the physical singularity time. Another important property of our model equation is that it can be computed efficiently. In particular, we show that when using a special parametrization, our model equation can be expressed in terms of the Riesz transform, which is a convolution operator. Thus it can be evaluated with the fast Fourier transform with $O(N^2\log(N))$ operation count. This offers a tremendous saving over the full equation and enables us to perform well-resolved computations to study the singularity formation of 3-D vortex sheets.

### A. Formulation

In this subsection, we will derive our 3-D vortex sheet model equation. From the stability analysis of Hou and Zhang,[13] we know that the leading order contribution of the integral on the right-hand side of Eq. (8) is the near field interaction in the neighborhood of $\mathbf{z}(\alpha)$. Since we expect that the vortex sheet surface is differentiable at the singularity, we propose to approximate

$$\mathbf{z}(\alpha,t)-\mathbf{z}(\alpha',t)$$

by the first order Taylor expansion around $\mathbf{z}(\alpha',t)$,

$$\mathbf{z}_{\alpha_1}(\alpha',t)(\alpha_1-\alpha_1')+\mathbf{z}_{\alpha_2}(\alpha',t)(\alpha_2-\alpha_2').$$

Consequently, the 3-D vortex sheet equation (9) becomes

$$\frac{\partial \mathbf{z}}{\partial t}(\alpha,t)=\int |\nabla_\alpha \mu(\alpha')^T,\nabla_\alpha \mathbf{z}(\alpha',t)^T|\frac{\mathbf{z}_{\alpha_1}(\alpha',t)(\alpha_1-\alpha_1')+\mathbf{z}_{\alpha_2}(\alpha',t)(\alpha_2-\alpha_2')}{|\mathbf{z}_{\alpha_1}(\alpha',t)(\alpha_1-\alpha_1')+\mathbf{z}_{\alpha_2}(\alpha',t)(\alpha_2-\alpha_2')|^3}d\alpha', \tag{113}$$

which can be further simplified as

$$\frac{\partial \mathbf{z}}{\partial t}(\alpha,t)=\frac{1}{4\pi}\int\int \frac{(\mu'_{\alpha_1}(\alpha_1-\alpha_1')+\mu'_{\alpha_2}(\alpha_2-\alpha_2'))(\mathbf{z}'_{\alpha_1}\times\mathbf{z}'_{\alpha_2})(\alpha',t)}{|\mathbf{z}'_{\alpha_1}(\alpha_1-\alpha_1')+\mathbf{z}'_{\alpha_2}(\alpha_2-\alpha_2')|^3}d\alpha_1'd\alpha_2', \tag{114}$$

where $\mathbf{z}'=\mathbf{z}(\alpha',t)$, $\mu'=\mu(\alpha')$. In order to evaluate the integral in the model equation (114) efficiently, we would like to reduce the above integral to a convolution operator. To this end, we would like to find a coordinate system $(\alpha_1,\alpha_2)$, such that

$$\mathbf{z}_{\alpha_1}\cdot\mathbf{z}_{\alpha_2}=C_1(t)\mathbf{z}_{\alpha_2}\cdot\mathbf{z}_{\alpha_2}, \tag{115}$$

$$\mathbf{z}_{\alpha_1}\cdot\mathbf{z}_{\alpha_1}=C_2(t)\mathbf{z}_{\alpha_2}\cdot\mathbf{z}_{\alpha_2}, \tag{116}$$

where $C_1(t)$ and $C_2(t)$ are independent of $\alpha_1$ and $\alpha_2$. The construction of such a spectral coordinate system will be provided in Sec. V B. With the choice of this coordinate system, the integral on the right-hand side of Eq. (114) can be expressed in terms of the convolution operators,

$$\frac{1}{2}\left(\tilde{H}_1\left(\frac{\mathbf{z}_{\alpha_1}\times\mathbf{z}_{\alpha_2}}{|\mathbf{z}_{\alpha_2}|^3}\mu_{\alpha_1}\right)+\tilde{H}_2\left(\frac{\mathbf{z}_{\alpha_1}\times\mathbf{z}_{\alpha_2}}{|\mathbf{z}_{\alpha_2}|^3}\mu_{\alpha_2}\right)\right), \tag{117}$$

where

$$\widetilde{H_k}(f)=\frac{1}{2\pi}\int \frac{(\alpha_k-\alpha_k')f(\alpha')d\alpha'}{[C_2(\alpha_1-\alpha_1')^2+2C_1(\alpha_1-\alpha_1')(\alpha_2-\alpha_2')+(\alpha_2-\alpha_2')^2]^{3/2}}, \tag{118}$$

with $k=1,2$. The exact Fourier symbols of these Riesz transforms can be written down explicitly as follows:[13]

$$\widehat{H_1}(\xi_1,\xi_2)=\frac{-i(\xi_1-C_1\xi_2)}{(C_2-C_1^2)(\xi_1^2-2C_1\xi_1\xi_2+C_2\xi_2^2)^{1/2}}, \tag{119}$$

and

$$\widehat{H_2}(\xi_1,\xi_2)=\frac{-i(C_2\xi_2-C_1\xi_1)}{(C_2-C_1^2)(\xi_1^2-2C_1\xi_1\xi_2+C_2\xi_2^2)^{1/2}}. \tag{120}$$

Since the Riesz transforms, $\widetilde{H_k}$, can be evaluated by fast Fourier transform, the complexity in evaluating the model equation (117) in each time step is reduced to $O(N^2\log N)$ from $O(N^4)$, where $N$ is the number of mesh points in each direction. Moreover, the constant in front of $O(N^2)$ is very small.

It is interesting to note that in the special case of 2-D vortex sheets, our model equation reduces to

$$\frac{\partial\overline{\mathbf{z}}}{\partial t}=\frac{1}{2i}H\left(\frac{\gamma}{\mathbf{z}_\alpha}\right), \tag{121}$$

where $\mathbf{z}=x(\alpha,t)+iy(\alpha,t)$ is the complex interface position, $\gamma=\mu_\alpha$ is the time independent vortex sheet strength, $H$ is the Hilbert transform, $H(f)=1/\pi\int f[(\alpha')/(\alpha-\alpha')]\,d\alpha'$. Using a similar approximation by Caflisch and Semmes,[12] we can rederive the local hyperbolic system of Caflisch and Semmes.[12] Moreover, in Hu's Ph.D. thesis,[23] he has performed extensive analytical and numerical studies to show that our 2-D model equation captures the same type of curvature singularities of order 3/2 as the full 2-D vortex sheet equation. Further, Hu[23] showed that our 2-D model equation captures the subtle disparity behavior between the singularity in the $x$ variable and that in the $y$ variable observed by Shelley[5] for certain initial data.

Before we perform our numerical study using the above 3-D model equation for vortex sheets, it is important to understand whether or not our model equation can capture the same singularity structure of the full 3-D vortex sheet equation. That is the topic of the next subsection, where we show that our model equation does capture the singularity type of the full equation, while the physical singularity time and location could be different.

### B. Early time singularity formation

Our goal in this subsection is to show that our three-dimensional model equation preserves the singularity type of the full three-dimensional vortex sheet equation. We consider a vortex sheet interface $\Gamma$ separating two layers of fluids. We parametrize the interface by

$$\mathbf{z}(\alpha_1,\alpha_2,t)=(x(\alpha_1,\alpha_2,t),y(\alpha_1,\alpha_2,t),z(\alpha_1,\alpha_2,t))^T,$$

and assume that the coordinates $(\alpha_1,\alpha_2)$ satisfy

$$\mathbf{z}_{\alpha_1}\cdot\mathbf{z}_{\alpha_2}=0,\quad \frac{\partial\mu}{\partial\alpha_1}=1,\quad \frac{\partial\mu}{\partial\alpha_2}=0, \tag{122}$$

at time $t=0$. Further, we assume that $\mathbf{z}$ is a small perturbation from the flat equilibrium solution, i.e., $|\mathbf{z}-(\alpha_1,\alpha_2,0)|\ll 1$.

In the previous section, we have shown that by considering $\alpha_2$ as a parameter and complexifying $\alpha_1$, $\mathbf{z}(\alpha_1,\cdot)$ develops singularities of order 3/2 on the $\alpha_1$-direction at $t=0+$. The key to this result is to derive a local term from the differential-integral equation. For the full 3-D vortex sheet equation, we have shown that the interface velocity can be written as

$$V(\alpha,t)=-V_{\mathrm{loc}}(\alpha,t)+V_1(\alpha,t), \tag{123}$$

$$=V_{\mathrm{loc}}(\alpha,t)+V_2(\alpha,t), \tag{124}$$

where

$$V_{\mathrm{loc}}=\frac{\mathbf{z}_{\alpha_1}}{2|\mathbf{z}_{\alpha_1}|^2}, \tag{125}$$

at $t=0$, and $V_1$, $V_2$ stand for the limiting velocity approaching from the upper and lower layer fluid, respectively.

Furthermore, the local term $2V_{\mathrm{loc}}$ represents a tangential velocity jump from the upper layer limiting velocity to the lower layer limiting velocity across the sheet. We found that the jump in tangential velocity fields is the driving force of the development of vortex sheet singularities. To derive a similar local approximate system for our model equation, we analyze the difference between the right-hand side of the full equation and that of our model equation. We will show that the difference is a regular integral and does not generate any discontinuity when extended into the complex $\alpha_1$ domain.

Define

$$u^f(\alpha,t)=-\frac{1}{4\pi}\int\int |\nabla_\alpha\mu(\alpha')^T,\nabla_\alpha\mathbf{z}(\alpha',t)^T| \times\frac{\mathbf{z}(\alpha,t)-\mathbf{z}(\alpha',t)}{|\mathbf{z}(\alpha,t)-\mathbf{z}(\alpha',t)|^3}d\alpha',$$

and

$$u^{\mathrm{mod}}(\alpha)=-\frac{1}{4\pi}\int\int |\nabla_\alpha\mu(\alpha')^T,\nabla_\alpha\mathbf{z}(\alpha',t)^T| \times\frac{\mathbf{z}_{\alpha_1}(\alpha',t)(\alpha_1-\alpha_1')+\mathbf{z}_{\alpha_2}(\alpha',t)(\alpha_2-\alpha_2')}{|\mathbf{z}_{\alpha_1}(\alpha',t)(\alpha_1-\alpha_1')+\mathbf{z}_{\alpha_2}(\alpha',t)(\alpha_2-\alpha_2')|^3}d\alpha',$$

where

$$|\nabla_\alpha\mu^T,\nabla_\alpha\mathbf{z}^T|=\frac{\partial\mu}{\partial\alpha_1}\mathbf{z}_{\alpha_2}-\frac{\partial\mu}{\partial\alpha_2}\mathbf{z}_{\alpha_1}.$$

The difference is

$$\begin{aligned}\mathrm{Diff}(\alpha,t) &= (u^f - u^{\mathrm{mod}})(\alpha,t)\\ &= -\frac{1}{4\pi}\int\int |\nabla_\alpha \mu(\alpha')^T, \nabla_\alpha \mathbf{z}(\alpha',t)^T|\\ &\quad \times K(\alpha,\alpha',t)\,d\alpha',\end{aligned}$$

where

$$\begin{aligned}K(\alpha,\alpha',t) &= \frac{\mathbf{z}(\alpha,t)-\mathbf{z}(\alpha',t)}{|\mathbf{z}(\alpha,t)-\mathbf{z}(\alpha',t)|^3}\\ &\quad - \frac{\mathbf{z}_{\alpha_1}(\alpha',t)(\alpha_1-\alpha_1') + \mathbf{z}_{\alpha_2}(\alpha',t)(\alpha_2-\alpha_2')}{|\mathbf{z}_{\alpha_1}(\alpha',t)(\alpha_1-\alpha_1') + \mathbf{z}_{\alpha_2}(\alpha',t)(\alpha_2-\alpha_2')|^3}.\end{aligned}$$

For initial data which are small analytic perturbations to the equilibrium, we can show that

$$\lim_{\alpha'\to\alpha} K(\alpha,\alpha',t) \leqslant \frac{A}{|\alpha-\alpha'|^{3/2}} \tag{126}$$

for $\alpha_2$ real and $|\mathrm{Im}(\alpha_1)|$ small. The above estimate holds up to the singularity time. This estimate implies that the kernel $K(\alpha,\alpha')$ is integrable, and the integral is continuous in $\alpha$. Therefore, there will be no jump on the integral when moving from one side of the real $\alpha_1$-axis to the other side of the real $\alpha_1$-axis.

Moreover, we can show that if the vortex sheet is an order $O(\epsilon)$ perturbation to equilibrium, $\mathrm{Diff}(\alpha,t)$ contains only higher order $O(\epsilon^2)$ contributions. In other words, our model equation captures all the leading order contributions of the full 3-D vortex sheet. Since the analysis is quite technical, we would not present it here. Our numerical experiments indicate that $\mathrm{Diff}(\alpha,t)$ is half order smoother than $u^f$ or $u^{\mathrm{mod}}$ even if $\mathbf{z}$ develops singularities of order 3/2. See the arguments after Eq. (94). A variant of this result has been proved by Caflisch and Semmes[12] for 2-D vortex sheets. This is also supported by our numerical experiments for analytic functions with singularities of order 3/2.

To derive a local approximate system for the model equation, we express the velocity field in terms of the velocity field of the full 3-D vortex sheet equation and the difference operator, $\mathrm{Diff}(\alpha,t)$:

$$V^{\mathrm{mod}} = V^f - \mathrm{Diff},$$

where $V^{\mathrm{mod}}$ is the velocity evaluated from the model equation. Using Eqs. (124) and (123), we obtain

$$V^{\mathrm{mod}} = -V_{\mathrm{loc}} + V_1 - \mathrm{Diff}, \tag{127}$$

$$= V_{\mathrm{loc}} + V_2 - \mathrm{Diff}. \tag{128}$$

Since Diff is continuous across the real $\alpha_1$ axes, Diff does not contribute any jump in the tangential velocity fields. Thus the model equation and the full equation generate the same jump in the tangential velocity fields. Moreover, since Diff is smaller and smoother than the leading order contribution, $V_{\mathrm{loc}}$, we obtain the same local approximate system for our model equation as that for the full vortex sheet equation. Thus the analysis we developed for the early time singularity for the full 3-D vortex sheet equation applies to our model equation. Consequently these two equations develop the same type of singularities at almost identical location up to the leading order term at $t=0^+$. However, it is important to note that the trajectories of the singularities in the extended $\alpha_1$ domain for the model equation are different from those for the full vortex sheet equation. This is because the lower order terms also contribute to the propagation of the singularity trajectories.

### C. Local form of the curvature singularity

In this subsection, we show that our model equation preserves the same local form of the curvature singularity near physical singularity time as the full vortex sheet equation.

From the analysis presented in the previous section, it is sufficient to show that we can derive the asymptotic system (92)–(94) from the model equation. Following the derivation by Hou and Zhang,[13] we can show that as long as the perturbations are small in magnitude, the difference between our model equation and the full equation only contributes to smoother or smaller terms. Thus, the leading order system from our model equation has exactly the same leading order terms as (92)–(94). Following the same derivations in Sec. III D, we can show that by the same transformation on the interface variables, our model equation preserves the same local form of the curvature singularity near physical singularity time.

## V. NUMERICAL STUDY

In this section, we confirm our theoretical analysis by performing numerical computations on three-dimensional vortex sheet problems. After briefly reviewing the formulation for our model equation, we will discuss some implementation issues and outline the computational algorithm. Our detailed numerical experiments confirm several aspects of our analytical results and provide strong evidence that singularities of order 3/2 develop for 3-D vortex sheets at some isolated points. Moreover the solution is more singular in the $\beta_1$ direction than in the $\beta_2$ direction.

### A. Formulation

In this subsection, we would like to further simplify our 3-D model equation derived in the previous section so that it can be computed more efficiently. As we can see, the integral in the model equation (114) is not a convolution operator in its present form. If we use direct numerical summation in our evaluation of the velocity integral, it would take $O(N^4)$ computational complexity in each time step, where $N$ is the number of mesh points in each direction. The numerical calculation becomes prohibitively expensive even when $N$ reaches the level of $O(100)$. To be able to efficiently evaluate the velocity on the right-hand side of the equation, we introduce a special coordinate system $(\alpha_1,\alpha_2)$ to reduce the integral operator in (114) to a convolution operator, so that fast Fourier transform can be used to evaluate the integral operator efficiently.

The special coordinate system is chosen so that Eqs. (115)–(116) are satisfied. With this set of coordinates, the

integral on the right-hand side of Eq. (114) becomes a convolution operator with the kernel

$$\frac{\alpha_i}{2\pi(C_2\alpha_1^2+2C_1\alpha_1\alpha_2+\alpha_2^2)^{3/2}}, \tag{129}$$

where $i=1,2$. In particular, when $C_1=0$ as in the case of our computation, the spectral representations of these two Riesz transforms become

$$\frac{-i\xi_1}{C_2(\xi_1^2+C_2\xi_2^2)^{1/2}}, \tag{130}$$

and

$$\frac{-i\xi_2}{(\xi_1^2+C_2\xi_2^2)^{1/2}}, \tag{131}$$

respectively. For an interface near equilibrium, it is possible to prove the existence of a set of coordinates satisfying (115)–(116) by a fixed point iteration [see (138)–(139)]. From our numerical experiences, we find that such coordinates exist even for large initial data.

### B. Some implementation issues

In this subsection, we discuss several implementation issues for our computations. The most important issue is how to construct a coordinate system that satisfies Eqs. (115)–(116) for all time. We divide this into two steps.

#### 1. Step 1: Initial orthogonal system

Initially, we need to find a system of $(\alpha_1,\alpha_2)$ such that Eqs. (115)–(116) are satisfied. We can derive a system of PDEs for these coordinates which can be solved by an iteration method.

Specifically, if the surface we consider is given by

$$\mathbf{z}=(x,y,\eta(x,y))$$

with $x$ and $y$ being the two parameters, we want to find a mapping $(x,y)\Rightarrow(\beta_1,\beta_2)$ such that Eqs. (115)–(116) are satisfied. Suppose we have

$$x=\beta_1+S_1(\beta_1,\beta_2), \tag{132}$$

$$y=\beta_2+S_2(\beta_1,\beta_2), \tag{133}$$

where $S_1$ and $S_2$ are periodic in $\beta$. By the chain rule, we get

$$\begin{aligned}\mathbf{z}_{\beta_1}&=(x_{\beta_1},y_{\beta_1},\eta_x x_{\beta_1}+\eta_y y_{\beta_1})\\&=(1+S_{1,\beta_1},S_{2,\beta_1},\eta_x(1+S_{1,\beta_1})+\eta_y S_{2,\beta_1}),\\ \mathbf{z}_{\beta_2}&=(x_{\beta_2},y_{\beta_2},\eta_x x_{\beta_2}+\eta_y y_{\beta_2})\\&=(S_{1,\beta_2},1+S_{2,\beta_2},\eta_x S_{1,\beta_2}+\eta_y(1+S_{2,\beta_2})).\end{aligned}$$

Thus, substituting these equations into (115)–(116) we get the coupled equations for $S_1$ and $S_2$:

$$\begin{aligned}\frac{\partial S_1}{\partial\beta_2}+\frac{\partial S_2}{\partial\beta_1}&=C_1(\mathbf{z}_{\beta_2}\cdot\mathbf{z}_{\beta_2})-(\mathbf{z}_{\beta_1}\cdot\mathbf{z}_{\beta_2}-S_{1,\beta_2}-S_{2,\beta_1})\\&\equiv F_1,\end{aligned} \tag{134}$$

$$\begin{aligned}\frac{\partial S_1}{\partial\beta_1}-C_2\frac{\partial S_2}{\partial\beta_2}&=\left(S_{1,\beta_1}-\frac{\mathbf{z}_{\beta_1}\cdot\mathbf{z}_{\beta_1}}{2}\right)\\&\quad-C_2\left(S_{2,\beta_2}-\frac{\mathbf{z}_{\beta_2}\cdot\mathbf{z}_{\beta_2}}{2}\right)\\&\equiv F_2,\end{aligned} \tag{135}$$

where

$$C_1=\frac{\langle\mathbf{z}_{\beta_1}\cdot\mathbf{z}_{\beta_2}\rangle}{\langle\mathbf{z}_{\beta_2}\cdot\mathbf{z}_{\beta_2}\rangle},\quad C_2=\frac{\langle\mathbf{z}_{\beta_1}\cdot\mathbf{z}_{\beta_1}\rangle}{\langle\mathbf{z}_{\beta 2}\cdot\mathbf{z}_{\beta 2}\rangle},$$

with $\langle f\rangle=(1/4\pi)^2\int f(\beta)d\beta$. Further, by differentiating (134) and (135) with respect to $\beta_1$ and $\beta_2$ and with some manipulations, we can derive the following couple system of elliptic equations for $S_1$ and $S_2$:

$$\frac{\partial^2 S_1}{\partial^2\beta_1}+C_2\frac{\partial^2 S_1}{\partial^2\beta_2}=C_2\frac{\partial F_1}{\partial\beta_2}+\frac{\partial F_2}{\partial\beta_1}, \tag{136}$$

$$\frac{\partial^2 S_2}{\partial^2\beta_1}+C_2\frac{\partial^2 S_2}{\partial^2\beta_2}=\frac{\partial F_1}{\partial\beta_1}-\frac{\partial F_2}{\partial\beta_2}. \tag{137}$$

For surfaces which are small perturbations from a flat surface, the existence of $S_1$ and $S_2$ can be proved by a fixed point iteration. However, we found from our numerical study that such a coordinate system exists generically for more general surfaces. In practice, we also solve for $S_1$ and $S_2$ by the same iterative method. Specifically, the iteration scheme is given as follows:

$$\frac{\partial^2 S_1^{n+1}}{\partial^2\beta_1}+C_2^n\frac{\partial^2 S_1^{n+1}}{\partial^2\beta_2}=C_2^n\frac{\partial F_1^n}{\partial\beta_2}+\frac{\partial F_2^n}{\partial\beta_1}, \tag{138}$$

$$\frac{\partial^2 S_2^{n+1}}{\partial^2\beta_1}+C_2^n\frac{\partial^2 S_2^{n+1}}{\partial^2\beta_2}=\frac{\partial F_1^n}{\partial\beta_1}-\frac{\partial F_2^n}{\partial\beta_2}, \tag{139}$$

where

$$C_1^n=\frac{\langle\mathbf{z}_{\beta_1}^n\cdot\mathbf{z}_{\beta_2}^n\rangle}{\langle\mathbf{z}_{\beta_2}^n\cdot\mathbf{z}_{\beta_2}^n\rangle},\quad C_2^n=\frac{\langle\mathbf{z}_{\beta_1}^n\cdot\mathbf{z}_{\beta_1}^n\rangle}{\langle\mathbf{z}_{\beta 2}^n\cdot\mathbf{z}_{\beta 2}^n\rangle}.$$

Here $\mathbf{z}_{\beta_i}^n$, $F_i^n$, etc., stand for the functions obtained using the $n$th iterative solution $S_i^n$ $(i=1,2)$. These quasi-Poisson equations for $S_1$ and $S_2$ are easily solved using FFT. For many examples we have considered, such an iterative scheme converges rapidly. It takes only a few iterations to reduce the iterative error to the order of $10^{-10}$. The same idea can also be applied to more general surfaces which are parametrized by $\mathbf{z}=(x(\alpha),y(\alpha),z(\alpha))$.

#### 2. Step 2: Enforcing (115)–(116) dynamically

During the evolution, it is possible that the coordinates from the last time-step do not satisfy Eqs. (115)–(116) in the current time-step. To avoid re-adjusting the coordinates every time-step, we add two tangential velocities to the evolution equation. These two added tangential velocities are determined by a set of linear elliptic PDE's to guarantee that Eqs. (115)–(116) are satisfied for all time.

As we know, the shape of the interface is determined solely by its normal velocity $\mathbf{w}\cdot\mathbf{n}$. Let $(T^1,T^2)$ denote the tangential velocity fields to be added to the original interface equation so that Eqs. (115)–(116) are satisfied for all time. The governing equation for the interface now takes the form of Eq. (10).

For any given time, we can derive a system of linear elliptic equations for $T^1$ and $T^2$ to satisfy Eqs. (115)–(116). Since the derivation of the elliptic system is quite technical, we defer it to Appendix B.

In the previous section, we have shown that the model equation generates the same type of branch point singularities at the extended complex domain as the full 3-D vortex sheet equation at $t=0+$. If we use the same reparametrization given by (115)–(116) for both the model equation and the full 3-D vortex sheet equation, the solutions of these two equations still have the same singularity structure at $t=0+$ in the new parametrization. While it is possible that the reparametrization may introduce additional singularities of a different type in the extended complex domain, the analytic study of Caflisch, Ercolani, Hou and Landis[24] for the leading order hyperbolic system shows that an isolated singularity is generically a square root branch point and it is stable under dynamic evolution. A square root branch point singularity in the hyperbolic system studied by Caflisch *et al.*[24] corresponds to a singularity of order 3/2 in the interface position. Thus, without loss of generality, we may assume that branch point singularities of order 3/2 are generated at $t=0+$ for both the model equation and the full 3-D vortex sheet equation in the new parametrization $\beta$.

Note that the new parametrization does not change the tangential velocity jump. Moreover, the argument that the difference between the right-hand sides of the full vortex sheet equation and the model equation is smoother still applies with the new parametrization. Further, the reparametrization of the vortex sheet does not change the shape of the surface, and curvature is independent of parametrization. These considerations suggest that the model equation captures the leading order singularity structure of the full 3-D vortex sheet equation at the physical singularity time.

The modification of the tangential velocity changes the evolution equation of the dipole strength $\mu$, i.e., $\mu$ is not conserved with time anymore. The evolution equation of $\mu$ under the new added tangential velocities is now governed by Eq. (10).

We remark that after each small time-step evolution, even though we evolve the interface with the added tangential velocities, (115)–(116) might not be completely satisfied at the discrete level due to the numerical error. Therefore, we need to use a projection technique to ensure that (115)–(116) are exactly satisfied at every time step (see Ref. 25 for details).

#### 3. Algorithm

We can summarize our computational algorithm as follows.

(1) Given the initial interface $\mathbf{z}$, construct $(\beta_1,\beta_2)$ that satisfies (115)–(116).
(2) Evaluate the original interface velocity, $\mathbf{w}$, on the right-hand side of Eq. (114) using FFT.
(3) Compute the tangential velocities $T^1$ and $T^2$ on $\beta_1$ and $\beta_2$ directions using the original interface velocity $\mathbf{w}$.
(4) Evolve the interface and the dipole strength using a fourth order Adams–Bashforth method.
(5) Reconstruct the fluid interface based on the newly updated interface to satisfy (115)–(116) exactly in the discrete level.
(6) Compute the solution at the next time step from step (2).

### C. Numerical results

In this subsection, we perform careful numerical studies using our 3-D vortex sheet model to confirm our theoretical results obtained in the previous sections. In particular, we investigate three aspects of singularity formation in 3-D vortex sheets:

(1) Interface shape and the curvature.
(2) Singularity formation.
(3) Local singularity structure.

In our three-dimensional computations, we study two initial conditions. The first case corresponds to using an orthogonal coordinate, while the second case uses a nonorthogonal coordinate.

#### 1. Case 1: Orthogonal coordinates

In this study, we take the following initial data:

$$\mathbf{z}(t=0)=(\alpha_1,\alpha_2,\varepsilon_1\sin(\alpha_1-\varepsilon_2\sin(\alpha_2))), \tag{140}$$

where $\varepsilon_1=0.1$, and $\varepsilon_2=0.5$, with

$$\mu(\alpha_1,\alpha_2)=2\alpha_1. \tag{141}$$

For this initial condition, we solve the model equation with $N=64$, $N=128$, $N=256$, $N=512$ and $N=1024$, respectively, to ensure the convergence of our computations. Every time we double the mesh points, we reduce the time-step $\Delta t$ by half. As a result, $\Delta t$ ranges from 0.01 to 0.000625. As in numerical study for 2-D vortex sheets,[4,5] it is essential to control the growth of round-off error by using a Fourier filter. The Fourier filter is simply to set to zero all Fourier coefficients that are below a certain given tolerance. The filter tolerance level is set to $10^{-12}$ in our computations which use the standard double precision. Higher precision computations would be desirable especially if we want to obtain an accurate form-fit for the singularity. However, the computations using higher precisions become very expensive with our limited computing resources. So we only present the results using double precision arithmetics.

Specifically, our computations proceed as follows.

(1) Evolve the interface using $N=256$, $\Delta t=0.0025$ up to $t=1.00$.
(2) Double the mesh size, reduce the time step in half, and continue the computation up to $t=1.65$ with $N=512$ and $\Delta t=0.00125$.
(3) At time $t=1.45$, further double the mesh size, reduce the time step in half and compute up to $t=1.60$ with $N=1024$ and $\Delta t=0.000625$.

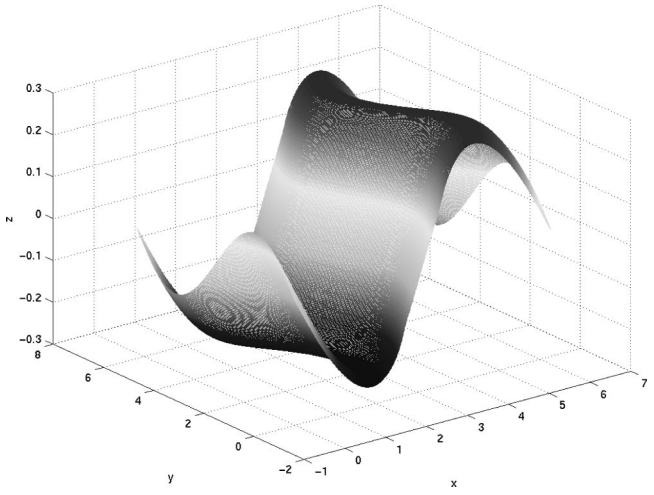


FIG. 1. Interface calculated from a three-dimensional model equation at $t=1.64$.

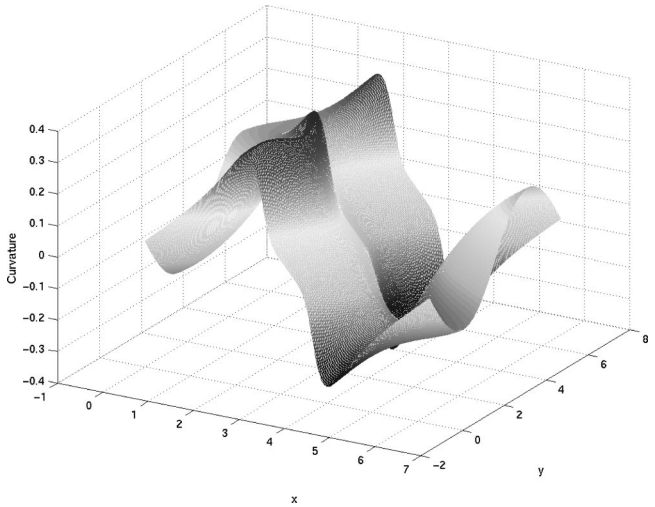


FIG. 3. Curvature calculated from a three-dimensional model equation at $t=1.400$.

We summarize our numerical results below.

(1) *Interface shape and the curvature plot.* In this part of the study, we illustrate the dynamical evolution of the sheet interface and its mean curvature. In Fig. 1, we plot the sheet interface at $t=1.64$. The interface looks quite smooth at this time although the curvature already develops some high gradient structures, see Fig. 4. We can see from Figs. 2–5 that the mean curvature develops a rapid growth in time and a curvature singularity may develop in finite time. It is important to point out that the initially smooth curvature function is pushed to form a sharp gradient along a certain direction (like the $\beta_1$ direction in our analysis in Sec. II B) while it remains relatively smooth perpendicular to this direction (like the $\beta_2$ direction in our analysis in Sec. II B). This confirms our analytic prediction that singularity formation for 3-D vortex sheets can be essentially reduced to a 2-D vortex sheet along a certain space curve. For these particular initial data, we have $\beta_1=\alpha_1$ and $\beta_2=\alpha_2$ according to (39)–(40).

In Sec. III, our analysis predicts that for each fixed $\beta_2$, singularities of order 3/2 form in the extended complex $\beta_1$ domain spontaneously at $t=0+$. Since the speeds at which the singularities propagate depend on $\beta_2$, we expect that the physical singularities would generically appear at some isolated points first, and then spread into a one-dimensional curve. In Fig. 6, we present the contour plot of the curvature. We can see that the singular region of curvature is indeed concentrated along a one-dimensional curve which is parametrized by $\beta_2$. The curvature achieves its maximum value at isolated points along these one-dimensional curves.

(2) *Singularity formation.* We study the singularity type in this part of the numerical study. Our purpose is to confirm that the singularity is of order 3/2 for a wide range of initial conditions along a certain direction. Following the work of Krasny,[4] we use the log–log plot of the

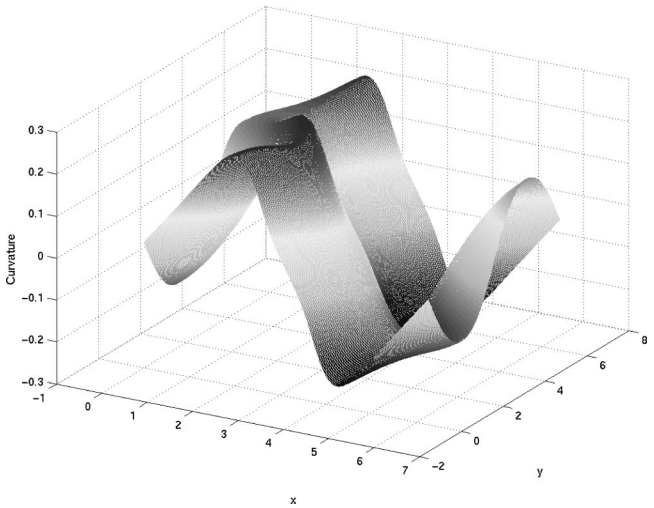


FIG. 2. Curvature calculated from a three-dimensional model equation at $t=1.20$.

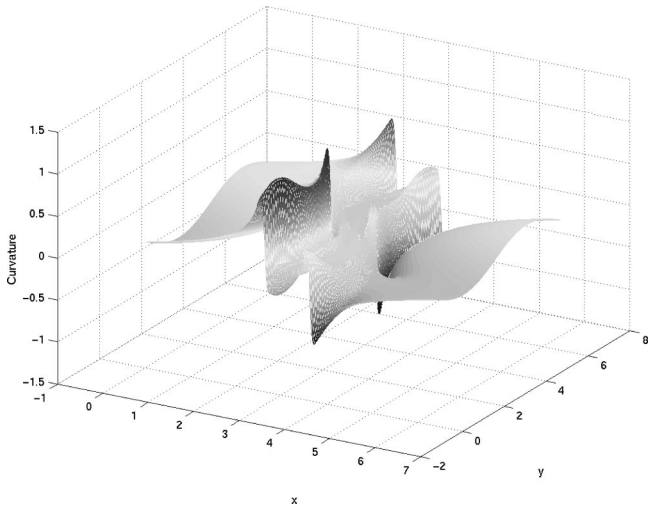


FIG. 4. Curvature calculated from a three-dimensional model equation at $t=1.60$.

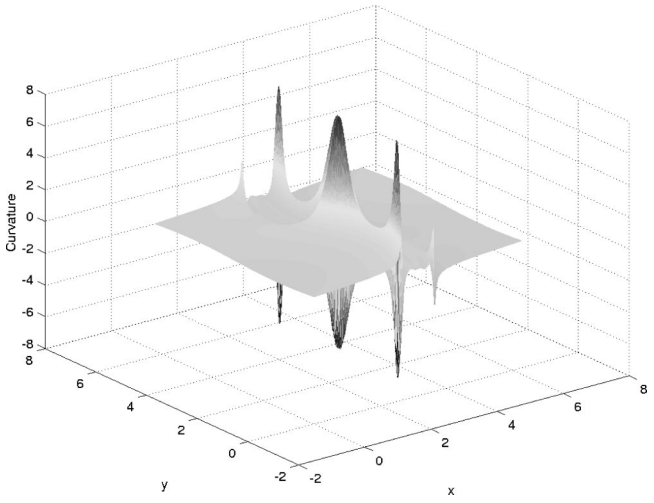


FIG. 5. Curvature calculated from a three-dimensional model equation at $t=1.646$.

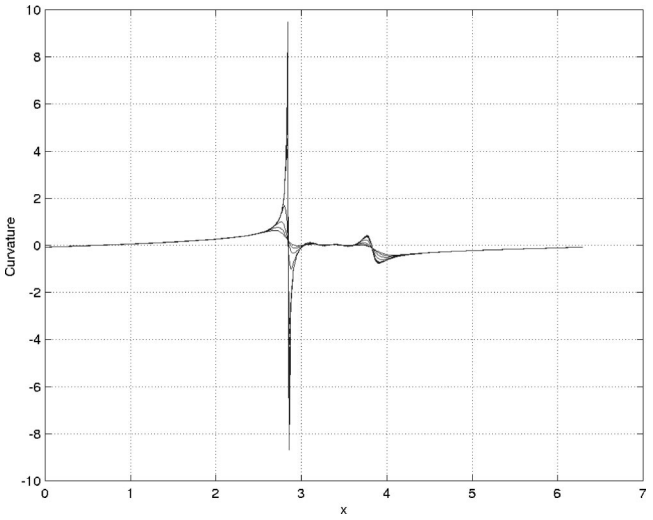


FIG. 7. Cross section of the curvature plot along $y=\pi$, at $t=1.2$, 1.3, 1.4, 1.5, 1.641–1.647, respectively.

Fourier coefficients of the $x$-component of the intersection along the $\beta_1$ direction with a fixed $\beta_2$. The $\beta_2$ is chosen such that the maximum curvature value is obtained at the intersection of these two directions. If the interface forms a singularity of order 3/2 at $t_c$ as predicted by our analysis, the slope of the logarithm of the Fourier modes would approach $-2.5$ asymptotically. In fact, from Figs. 7–10, we see that the Fourier modes are approaching the $-2.5$ slope as time increases. In particular, the four curves in Figs. 8–10 represent the Fourier modes at four different times. As the singularity time is approached, we can see that the Fourier modes corresponding to the lower to intermediate wave numbers converge to the $-2.5$ slope, while the higher wave number modes also move towards this slope as the singularity time is approached. In addition, we find that the $x$, $y$, and $z$ components form a singularity of order 3/2 simultaneously. This indicates that the interface may form a singularity of order 3/2 in finite time.

To provide further evidence of singularity formation of order 3/2, we have performed a careful resolution study. In Fig. 11, we present the numerical resolution study in the $x$ variable using $N=512$ and $N=1024$, respectively. In addition, Fig. 12 shows the close-up of the plot in Fig. 11 in the high frequency region. From the close-up picture, we observe that as soon as the logarithms of the Fourier modes deviate from the $-2.5$ slope, the curves representing the logarithms of the 512 by 512 computations also deviate from those in the 1024 by 1024 computations. Therefore, we conclude that the decaying behavior of the higher wave number modes in these figures is due to the lack of numerical resolution and the filtering effect. Moreover, we observe that at the same high wave number, the coefficients computed from higher resolution ($N=1024$) are closer to the $-2.5$ slope. This

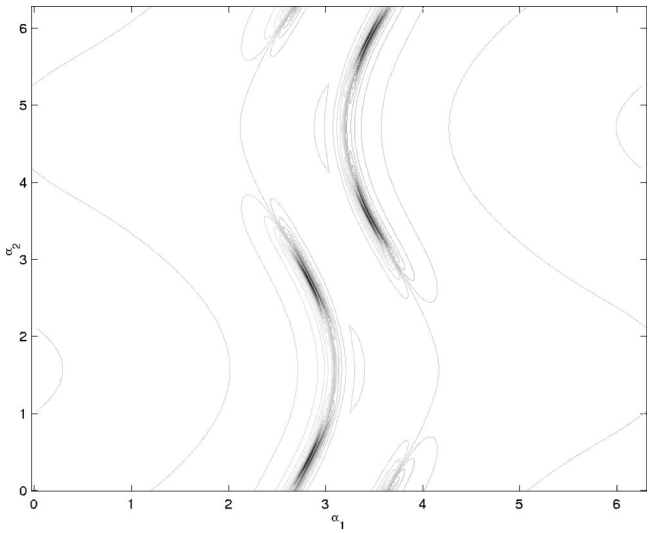


FIG. 6. Curvature contours calculated from a three-dimensional model equation at $t=1.646$.

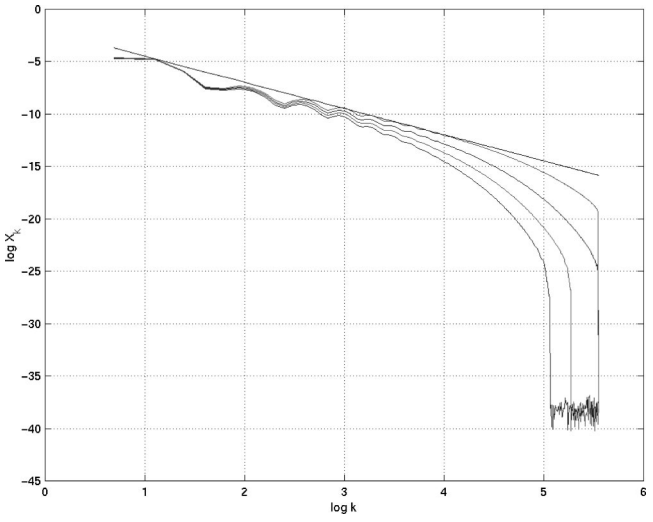


FIG. 8. Log–log plot of the Fourier coefficients in an $x$ variable along the $\alpha_1$-direction passing through the maximum curvature position at time $t=1.61$, 1.62, 1.63, 1.64. The Fourier coefficients increase as time increases. The straight line shows the $-2.5$ slope.

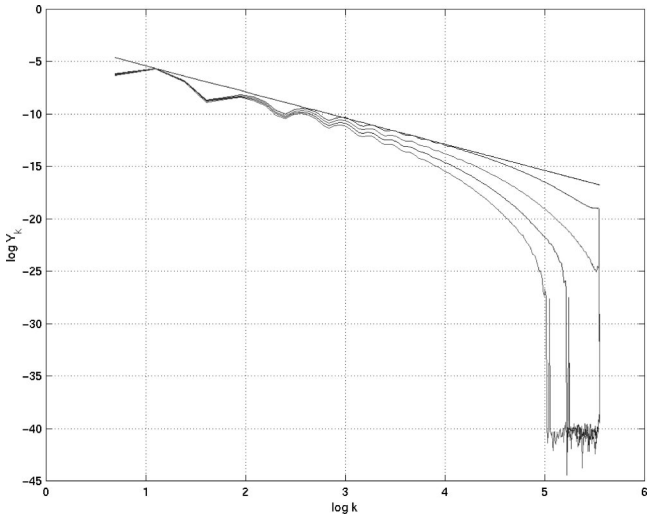


FIG. 9. Log–log plot of the Fourier coefficients in a $y$ variable along the $\alpha_1$-direction passing through the maximum curvature position at time $t=1.61, 1.62, 1.63, 1.64$. The Fourier coefficients increase as time increases. The straight line shows the $-2.5$ slope.

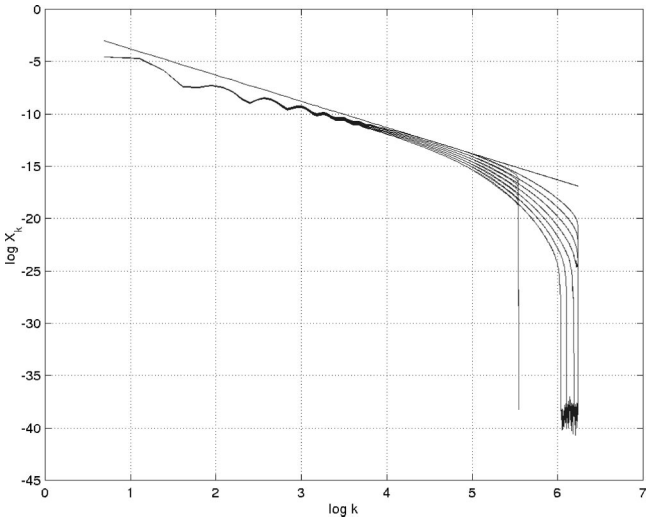


FIG. 11. Log–log plot of the Fourier coefficients in an $x$ variable along the $\alpha_1$-direction passing through the maximum curvature position at time $t=1.641$, to 1.647 at the interval of 0.001. The straight line shows the $-2.5$ slope. The two sets of curves correspond to computations using 512 mesh points and 1024 mesh points, respectively.

indicates that the higher wave number modes will eventually converge to the $-2.5$ slope as more and more mesh points are used. This resolution study gives some evidence that a singularity of order 3/2 is formed at the singularity time. Very similar behavior is observed for the $y$ and $z$ variables. Since the results are basically the same, we do not present them here.

We remark that to obtain a complete confirmation of the order of the singularity, one has to perform high resolution computations with high machine precisions, and use some sophisticated form-fitting technique; see, e.g., Shelley.[5] Unfortunately, due to the drastic increase of computational costs for the 3-D vortex sheet equation, we could not afford to perform such high resolution, high machine precision computations for the 3-D vortex sheet equation. This should be done and will be left for future work. Thus, our computational results presented in this paper provide only partial confirmation of the finite time singularity formation of 3-D vortex sheets. The results on the order of the singularities are consistent with our analytic prediction.

(3) *Local singularity structure.* In Sec. III D, in order to study the local singularity structure, we introduce two new variables $\phi_1$ and $\phi_2$. We show that to the leading order $\phi_2$ and $z$ form singularities of order 3/2 but there is no singularity of order 3/2 in the $\phi_1$ variable. Since our analysis is based on formal asymptotic analysis, we would like to confirm this result numerically. From the log–log plot of the Fourier coefficients of the $\phi_1$ and $\phi_2$

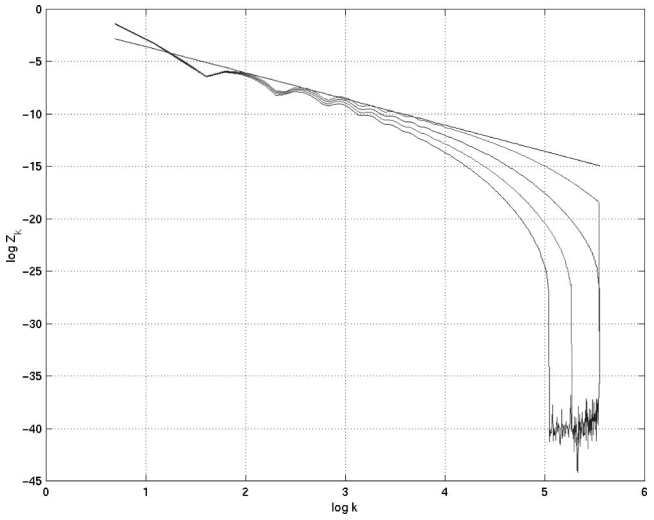


FIG. 10. Log–log plot of the Fourier coefficients in a $z$ variable along the $\alpha_1$-direction passing through the maximum curvature position at time $t=1.61, 1.62, 1.63, 1.64$. The Fourier coefficients increase as time increases. The straight line shows the $-2.5$ slope.

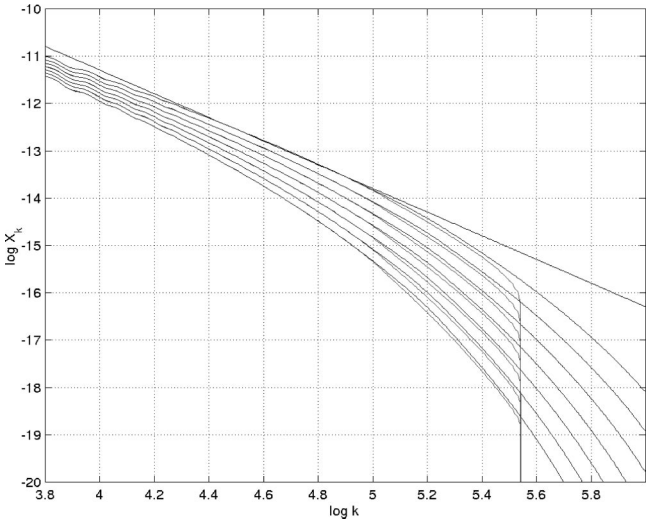


FIG. 12. Close-up plot of Fig. 11. Note that as soon as the logarithms of the Fourier modes deviate from the $-2.5$ slope, the curves corresponding to the 512 by 512 computations also deviate from those of the 1024 by 1024 computations.

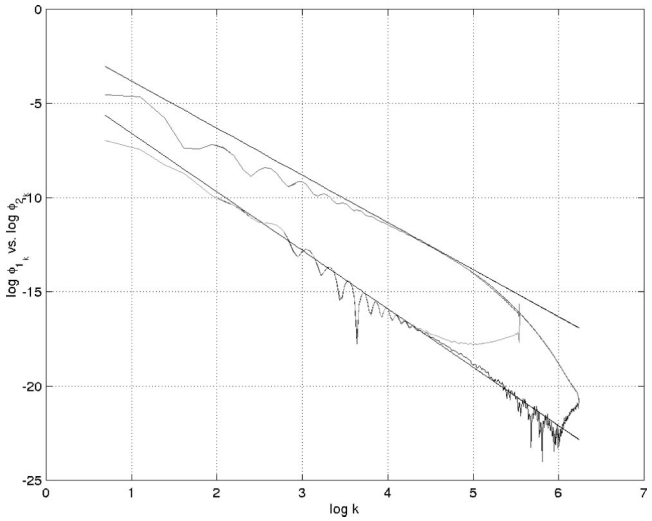


FIG. 13. A comparison of the log–log plot of the $\phi_1$ variable Fourier coefficients to that of the $\phi_2$ variable along the $\alpha_1$ direction. Both cross sections along $\alpha_1$ pass through the maximum curvature position at time $t=1.646$. The upper line corresponds to the Fourier coefficients of the $\phi_2$ variable, the straight line has the slope of $-2.5$. The lower line corresponds to the Fourier coefficients of the $\phi_1$ variable, the straight line has the slope of $-3.1$. Solutions are computed using $N=512$ and $N=1024$.

variables along the $\beta_1$ direction in Figs. 13 and 14, we see that the Fourier modes of the $\phi_1$ variable approaches the $-3.1$ slope, while the Fourier modes of the $\phi_2$ variable approaches the $-2.5$ slope. This confirms that $\phi_1$ is indeed smoother than $\phi_2$ near the singularity time.

Throughout our analysis, we argue that under the special set of coordinates, one direction is the essential singularity direction (the $\beta_1$ direction). In the case we study here, even with the added tangential velocities and the adjusted dipole strength, the $\beta_1$ direction corresponds to the $\alpha_1$-direction. So the $\alpha_1$-direction should be the essential singular direction to the leading order. To confirm this, we compare the Fourier coefficients of the solution along the $\alpha_1$-direction to the Fourier coefficients of the solution along the $\alpha_2$-direction. As we can see from Fig. 15, even though our $\varepsilon_1=0.1$ is not particularly small, there are still disparities in the tails of the Fourier coefficients in the $x$ variable. Almost the same behavior is observed for the $y$ and $z$ variables. This shows that the $\beta_1$ direction, which coincides with the $\alpha_1$-direction in this case, is the essential direction driving the singularity formation of the 3-D vortex sheet problem. We also present the same comparison at a later time in Fig. 16 which provides further evidence to support our analytical result.

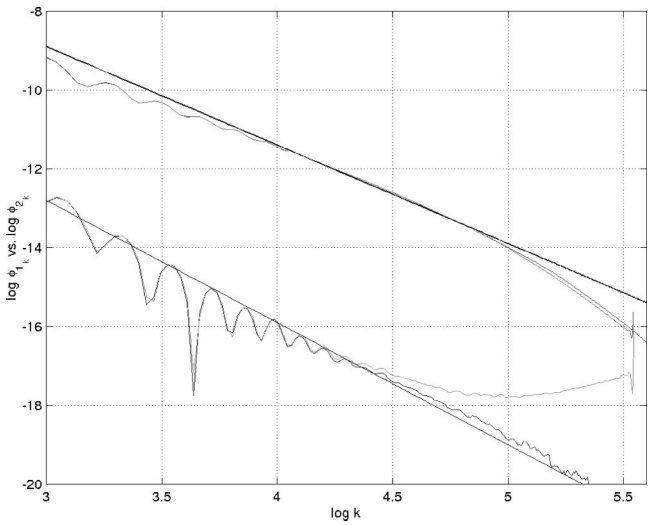


FIG. 14. Zoomed plot of Fig. 13. A comparison of the log–log plot of the $\phi_1$ variable Fourier coefficients to that of the $\phi_2$ variable. Both intersections pass the maximum curvature position at time $t=1.646$. The upper line is the Fourier coefficients of the $\phi_2$ variable, the straight line has the slope of $-2.5$. The lower line stands for the Fourier coefficients of the $\phi_1$ variable, the straight line has the slope of $-3.1$. Solutions are computed using $N=512$ and $N=1024$.

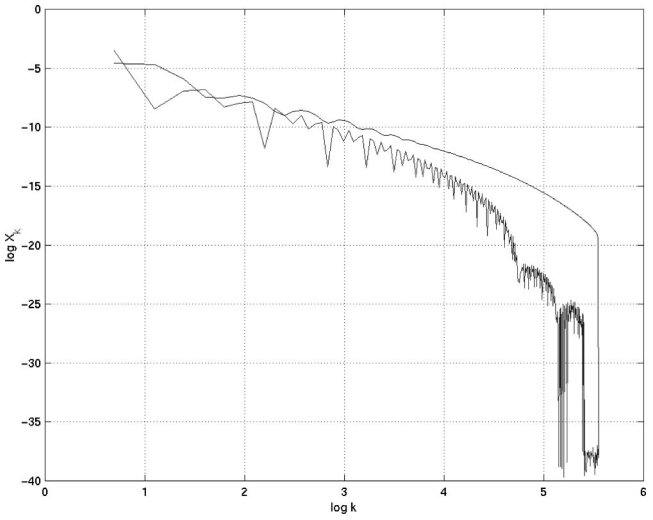


FIG. 15. A comparison of the log–log plot of the Fourier coefficients in an $x$ variable along the $\alpha_1$-direction with that along the $\alpha_2$-direction at $t=1.64$. The upper line corresponds to the Fourier coefficients along the $\alpha_1$-direction. The lower line corresponds to the Fourier coefficients along the $\alpha_2$-direction.

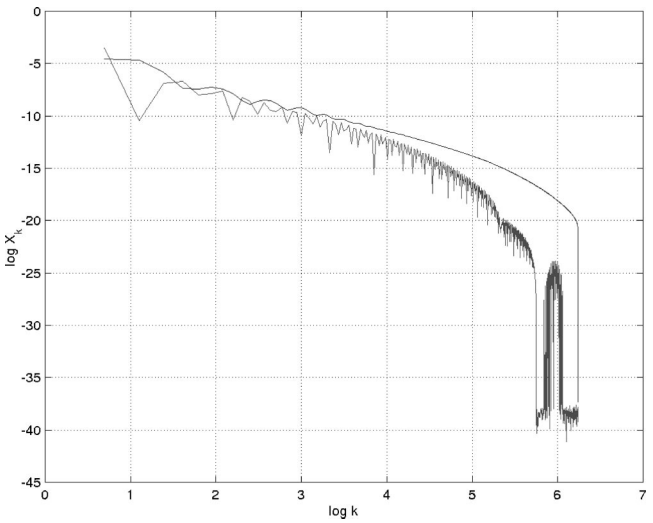


FIG. 16. A comparison of the log–log plot of the Fourier coefficients along the $\alpha_1$-direction with that along the $\alpha_2$ direction at $t=1.647$. The upper line corresponds to the Fourier coefficients along the $\alpha_1$-direction. The lower line corresponds to the Fourier coefficients along the $\alpha_2$-direction.

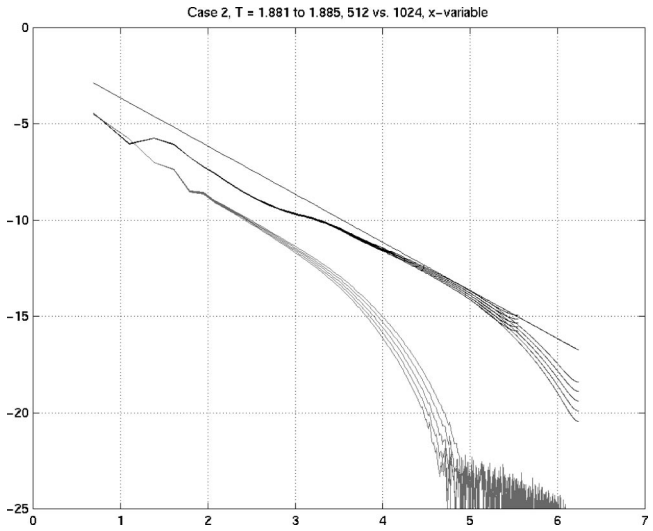


FIG. 17. Log–log plot of the Fourier coefficients in the $x$ variable along the $\beta_1$-direction versus the same Fourier coefficients along the $\beta_2$-direction. Both curves along both directions pass through the maximum curvature position at time $t=1.881$, to 1.885 at the interval of 0.001. The top curves correspond to the Fourier coefficients along the $\beta_1$ direction. The lower curves correspond to the Fourier coefficients along the $\beta_2$ direction. The straight line shows the $-2.5$ slope. The solutions are computed using $N=512$ and $N=1024$, respectively.

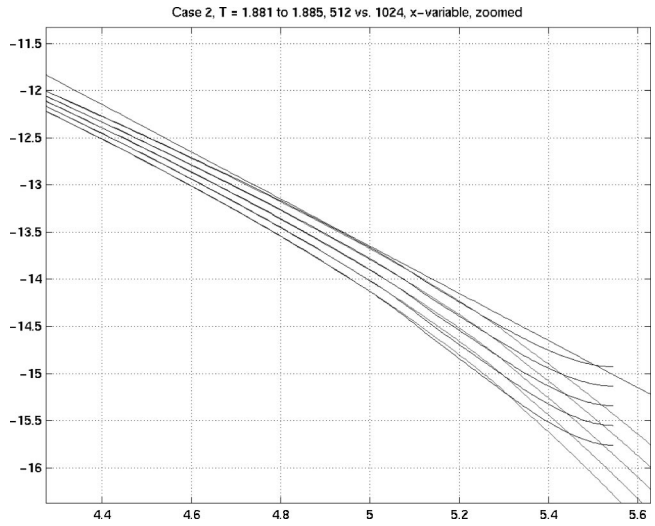


FIG. 18. The close-up of the top curves in Fig. 17 along the $\beta_1$ direction.

### 2. Case 2: Nonorthogonal coordinates

In our last example, there exists a set of coordinates that satisfy the equation with $C_1=0$. In addition, the tangential velocity jump direction coincides with one of the parameter direction. This makes the computation somewhat special. In our next example, the tangential velocity jump has the contributions in both $\alpha_1$ and $\alpha_2$ directions. Also, there is no orthogonal coordinates that satisfy Eqs. (115)–(116).

In this study, we choose the initial condition as

$$\mathbf{z}(t=0)=(\alpha_1,\alpha_2,\varepsilon_1\sin(\alpha_1-\varepsilon_2\sin(\alpha_2))), \tag{142}$$

where $\varepsilon_1=0.1$, and $\varepsilon_2=0.5$, with

$$\mu(\alpha_1,\alpha_2)=\alpha_1+\alpha_2. \tag{143}$$

In our computations, we use the mesh size of 256 and $\Delta t=0.0025$ to compute up to $t=1.500$, then to $t=1.825$ with a mesh size of 512 and $\Delta t=0.00125$, finally to $t=1.885$ with a mesh size of 1024 and $\Delta t=0.000625$. For these initial data, we have $\beta_1=\alpha_1+\alpha_2$, $\beta_2=\alpha_1-\alpha_2$, according to (39)–(40). To confirm our analysis for this case, we analyze the $\beta_1$ and $\beta_2$ intersections to compare their Fourier coefficients.

In Fig. 17, we present the log–log plot of the Fourier coefficients of the $x$ variable. Two sets of plots are generated, one along the $\beta_1$-direction with a fixed $\beta_2$, and the other along the $\beta_2$-direction with a fixed $\beta_1$. The fixed parameters, $\beta_1$ or $\beta_2$ are chosen so that the cross-section along the other direction passes the maximum curvature position at time $t=1.881$, to 1.885 at the interval of 0.001. As we can see, the Fourier coefficients increase as time increases. The straight line shows the $-2.5$ slope. The cluster of curves on the top corresponds to the Fourier coefficients along the $\beta_1$ direction, while the cluster of curves in the lower part corresponds to the Fourier coefficients along the $\beta_2$ direction. We can see that solution is clearly more singular along the $\beta_1$ direction than that along the $\beta_2$ direction.

In Fig. 18, we present a close-up of the Fourier coefficients along the $\beta_1$ direction presented in Fig. 17. To ensure that we have enough resolution, we have used two sets of numerical resolutions in this study, one with 512 by 512 mesh points, and in another with 1024 by 1024 mesh points. We can see that the Fourier coefficients converge to the slope $-2.5$ as time increases with increasing resolution. This is again consistent with our theoretical prediction given in the previous section. The same behavior has also been observed in the $y$ and $z$ variables. We do not present them here.

## ACKNOWLEDGMENTS

The research presented here was strongly motivated by a number of fruitful discussions with Dr. Stephen Cowley during his visit to Caltech in the summer of 1998. The fact that the 3-D vortex sheet singularity is supported in a locally thin region was first observed by Dr. Cowley using a different asymptotic analysis based on a scaling argument. We have also benefited from several inspiring conversations with Dr. Dale Pullin. We are indebted to Dr. Hector Ceniceros for his valuable suggestions regarding the presentation of the original manuscript. The research was in part supported by a grant from the National Science Foundation under Contract No. DMS-0073916, and by a grant from the Army Research Office under Contract No. DAAD19-99-1-0141. P.Z. also wishes to acknowledge the support of the Special Funds for Major State Basic Research Projects No. G1999032804 from China.

## APPENDIX A: LEADING ORDER EQUATION OF $\psi_3$

In this appendix, we will derive a leading order evolution equation for $\psi_3$. To this end, we substitute (25) and (26) into (35), and extract the leading order terms:

$$\begin{aligned}\frac{\partial \psi_3}{\partial t} = &-\frac{1}{4\pi}\int\int \frac{\gamma_1(-H_2(\psi_1')-H_1(\psi_2'))_{\alpha_2}(\alpha_2-\alpha_2')}{|\mathbf{z}-\mathbf{z}'|^3}+\frac{\gamma_2(H_2(\psi_1')+H_1(\psi_2'))_{\alpha_1}(\alpha_2-\alpha_2')}{|\mathbf{z}-\mathbf{z}'|^3}\\ &+\frac{\gamma_2(H_1(\psi_1')-H_2(\psi_2'))_{\alpha_1}(\alpha_1-\alpha_1')}{|\mathbf{z}-\mathbf{z}'|^3}-\frac{\gamma_1(H_1(\psi_1')-H_2(\psi_2'))_{\alpha_2}(\alpha_1-\alpha_1')}{|\mathbf{z}-\mathbf{z}'|^3}-\frac{\gamma_2(H_1(\psi_1-\psi_1')-H_2(\psi_2-\psi_2'))}{|\mathbf{z}-\mathbf{z}'|^3}\\ &-\frac{\gamma_1(-H_2(\psi_1-\psi_1')-H_1(\psi_2-\psi_2'))}{|\mathbf{z}-\mathbf{z}'|^3}-\frac{\gamma_1(\alpha_1-\alpha_1')+\gamma_2(\alpha_2-\alpha_2')}{|\mathbf{z}-\mathbf{z}'|^3}d\alpha'+O(\varepsilon^2),\end{aligned} \tag{A1}$$

where $\psi_i'=\psi_i(\alpha')$, $i=1,2$. By using (31) and the properties of the Riesz transforms (18)–(19), we obtain

$$\begin{aligned}\frac{\partial \psi_3}{\partial t} = &\frac{1}{2}\gamma_1 H_2^2 D_2\psi_1+\frac{1}{2}\gamma_1 H_2 H_1 D_2\psi_2-\frac{1}{2}\gamma_2 H_2^2 D_1\psi_1-\frac{1}{2}\gamma_2 H_2 H_1 D_1\psi_2+\frac{1}{2}\gamma_1 H_1^2 D_2\psi_1-\frac{1}{2}\gamma_1 H_1 H_2 D_2\psi_2\\ &-\frac{1}{2}\gamma_2 H_1^2 D_1\psi_1+\frac{1}{2}\gamma_2 H_1 H_2 D_1\psi_2+\frac{1}{2}\gamma_2\Lambda H_1\psi_1-\frac{1}{2}\gamma_2\Lambda H_2\psi_2-\frac{1}{2}\gamma_1\Lambda H_2\psi_1-\frac{1}{2}\gamma_1\Lambda H_1\psi_2\\ &+\frac{1}{4\pi}\int\frac{\gamma_2(\alpha_2-\alpha_2')+\gamma_1(\alpha_1-\alpha_1')}{|\mathbf{z}-\mathbf{z}'|^3}d\alpha'+O(\varepsilon^2)\\ =&\frac{1}{2}(\gamma_1 D_1+\gamma_2 D_2)\psi_2+\frac{1}{4\pi}\int\frac{\gamma_2(\alpha_2-\alpha_2')+\gamma_1(\alpha_1-\alpha_1')}{|\mathbf{z}-\mathbf{z}'|^3}d\alpha'+O(\varepsilon^2).\end{aligned} \tag{A2}$$

It is necessary to analyze the integral term of Eq. (A2) and extract the leading order contributions. By further expanding the integral in terms of $S_i$'s, we find that the leading order terms are

$$\begin{aligned}\frac{1}{4\pi}\int\frac{\gamma_2(\alpha_2-\alpha_2')+\gamma_1(\alpha_1-\alpha_1')}{|\mathbf{z}-\mathbf{z}'|^3}d\alpha' = &-\frac{3}{4\pi}\int\frac{\gamma_2(\alpha_2-\alpha_2')[(S_1-S_1')(\alpha_1-\alpha_1')+(S_2-S_2')(\alpha_2-\alpha_2')]}{|\mathbf{z}-\mathbf{z}'|^5}d\alpha'\\ &-\frac{3}{4\pi}\int\frac{\gamma_1(\alpha_1-\alpha_1')[(S_1-S_1')(\alpha_1-\alpha_1')+(S_2-S_2')(\alpha_2-\alpha_2')]}{|\mathbf{z}-\mathbf{z}'|^5}+O(\epsilon^2).\end{aligned} \tag{A3}$$

Using integration by parts and applying (18)–(19), we get

$$\begin{aligned}&\frac{1}{4\pi}\int\frac{\gamma_2(\alpha_2-\alpha_2')+\gamma_1(\alpha_1-\alpha_1')}{|\mathbf{z}-\mathbf{z}'|^3}d\alpha'\\ &=-\frac{1}{2}\gamma_2(H_1D_2(S_1)+(2H_2D_2+H_1D_1)(S_2))-\frac{1}{2}\gamma_1((2H_1D_1+H_2D_2)(S_1)+H_1D_2(S_2))+O(\varepsilon^2).\end{aligned} \tag{A4}$$

The above derivation is similar in spirit to that of Appendix B in the paper by Hou, Teng and Zhang.[26] By substituting (25) and (26) into (A4), we write the leading order terms in $\psi_1$ and $\psi_2$:

$$\begin{aligned}&\frac{1}{4\pi}\int\frac{\gamma_2(\alpha_2-\alpha_2')+\gamma_1(\alpha_1-\alpha_1')}{|\mathbf{z}-\mathbf{z}'|^3}d\alpha'\\ &=-\frac{1}{2}\gamma_2(H_1D_2)(-H_2\psi_1-H_1\psi_2)-\frac{1}{2}\gamma_2(2H_2D_2+H_1D_1)(H_1\psi_1-H_2\psi_2)\\ &\quad-\frac{1}{2}\gamma_1(2H_1D_1+H_2D_2)(-H_2\psi_1-H_1\psi_2)-\frac{1}{2}\gamma_1H_1D_2(H_1\psi_1-H_2\psi_2)+O(\varepsilon^2),\end{aligned} \tag{A5}$$

which can be further simplified to

$$\frac{1}{4\pi}\int \frac{\gamma_2(\alpha_2-\alpha_2')+\gamma_1(\alpha_1-\alpha_1')}{|\mathbf{z}-\mathbf{z}'|^3}d\alpha'$$

$$=-\frac{1}{2}(H_1D_1+H_2D_2)(-\gamma_1H_2+\gamma_2H_1)\psi_1+(H_1D_1+H_2D_2)(\gamma_1H_1+\gamma_2H_2)\psi_2+O(\varepsilon^2)$$

$$=-(\gamma_1D_1+\gamma_2D_2)\psi_2-\frac{1}{2}(\gamma_1D_2-\gamma_2D_1)\psi_1+O(\varepsilon^2). \tag{A6}$$

Thus we obtain the leading order evolution equation for $\psi_3$ as follows:

$$\frac{\partial\psi_3}{\partial t}=-\frac{1}{2}(\gamma_1D_1+\gamma_2D_2)\psi_2+\frac{1}{2}(\gamma_2D_1-\gamma_1D_2)\psi_1+O(\varepsilon^2). \tag{A7}$$

## APPENDIX B: DERIVATION OF EQUATIONS FOR $T^1$ AND $T^2$

In this appendix, we will derive the elliptic system for $T^1$ and $T^2$ so that Eqs. (115)–(116) are satisfied for all times.

Recall that

$$\mathbf{z}_{\beta_1}=|\mathbf{z}_{\beta_1}|\mathbf{t}_1,$$

$$\mathbf{z}_{\beta_2}=|\mathbf{z}_{\beta_2}|\mathbf{t}_2.$$

Note that

$$(C_1(t))^2<C_2(t), \tag{B1}$$

since

$$C_1(t)|\mathbf{z}_{\beta_2}|^2=\mathbf{z}_{\beta_1}\cdot\mathbf{z}_{\beta_2}<|\mathbf{z}_{\beta_1}|\cdot|\mathbf{z}_{\beta_2}|.$$

Thus we have

$$(C_1(t))^2<\frac{|\mathbf{z}_{\beta_1}|^2}{|\mathbf{z}_{\beta_2}|^2}=C_2(t).$$

Now define

$$\mathbf{t}_1\cdot\mathbf{t}_2=\frac{\mathbf{z}_{\beta_1}\cdot\mathbf{z}_{\beta_2}}{|\mathbf{z}_{\beta_1}|\cdot|\mathbf{z}_{\beta_2}|}=\frac{C_1(t)}{\sqrt{C_2(t)}}=\cos\theta,\quad 0<\theta<\pi. \tag{B2}$$

Suppose that we have constructed the initial coordinate system satisfying Eqs. (115)–(116) at $t=0$. To ensure that Eqs. (115)–(116) are satisfied for all time, we differentiate Eqs. (115)–(116) with respect to time. This gives

$$(\mathbf{z}_t)_{\beta_1}\cdot\mathbf{z}_{\beta_2}+\mathbf{z}_{\beta_1}\cdot(\mathbf{z}_t)_{\beta_2}=2C_1(t)(\mathbf{z}_t)_{\beta_2}\cdot\mathbf{z}_{\beta_2}+C_1'(t)|\mathbf{z}_{\beta_2}|^2, \tag{B3}$$

$$(\mathbf{z}_t)_{\beta_1}\cdot\mathbf{z}_{\beta_1}=C_2(t)(\mathbf{z}_t)_{\beta_2}\cdot z_{\beta_2}+\frac{C_2'(t)}{2}|\mathbf{z}_{\beta_2}|^2. \tag{B4}$$

Next, we introduce two new variables $T^3$ and $T^4$ as follows:

$$T^3=T^1+\cos\theta T^2, \tag{B5}$$

$$T^4=T^2+\cos\theta T^1. \tag{B6}$$

Then we have

$$T^1=\frac{1}{\sin^2\theta}(T^3-\cos\theta T^4), \tag{B7}$$

$$T^2=\frac{1}{\sin^2\theta}(T^4-\cos\theta T^3). \tag{B8}$$

Using the interface equation (10), we can reduce (B3)–(B4) to the following system:

$$|\mathbf{z}_{\beta_1}|T^3_{\beta_2}+|\mathbf{z}_{\beta_2}|T^4_{\beta_1}-2C_1(t)|\mathbf{z}_{\beta_2}|T^4_{\beta_2}$$
$$=-|\mathbf{z}_{\beta_2}|(\mathbf{t}_{1\beta_1}\cdot\mathbf{t}_2)T^1-|\mathbf{z}_{\beta_1}|(\mathbf{t}_{2\beta_1}\cdot\mathbf{t}_1)T^2$$
$$+2C_1(t)|\mathbf{z}_{\beta_2}|(\mathbf{t}_{1\beta_2}\cdot\mathbf{t}_2)T^1-|\mathbf{z}_{\beta_2}|\mathbf{w}_{\beta_1}\cdot\mathbf{t}_2-|\mathbf{z}_{\beta_1}|\mathbf{w}_{\beta_2}\cdot\mathbf{t}_1$$
$$+2C_1(t)|\mathbf{z}_{\beta_2}|\mathbf{w}_{\beta_2}\cdot\mathbf{t}_2+C_1'(t)|\mathbf{z}_{\beta_2}|^2, \tag{B9}$$

$$|\mathbf{z}_{\beta_1}|T^3_{\beta_1}-|\mathbf{z}_{\beta_2}|C_2(t)T^4_{\beta_2}$$
$$=C_2(t)|\mathbf{z}_{\beta_2}|(\mathbf{t}_{1\beta_2}\cdot\mathbf{t}_2)T^1-|\mathbf{z}_{\beta_1}|(\mathbf{t}_{2\beta_1}\cdot\mathbf{t}_1)T^2$$
$$+C_2(t)|\mathbf{z}_{\beta_2}|\mathbf{w}_{\beta_2}\cdot\mathbf{t}_2-|\mathbf{z}_{\beta_1}|\mathbf{w}_{\beta_1}\cdot\mathbf{t}_1+C_2'(t)\frac{|\mathbf{z}_{\beta_2}|^2}{2}. \tag{B10}$$

If we divide Eq. (B9) by $|\mathbf{z}_{\beta_2}|$ and Eq. (B10) by $|\mathbf{z}_{\beta_1}|$, we arrive at

$$\sqrt{C_2(t)}T^3_{\beta_2}+(T^4_{\beta_1}-2C_1(t)T^4_{\beta_2})=L_1+G_1+C_1'(t)|\mathbf{z}_{\beta_2}|, \tag{B11}$$

$$T^3_{\beta_1}-\sqrt{C_2(t)}T^4_{\beta_2}=L_2+G_2+C_2'(t)\frac{|\mathbf{z}_{\beta_2}|}{2}, \tag{B12}$$

where

$$L_1=-(\mathbf{t}_{1\beta_1}\cdot\mathbf{t}_2)T^1-\sqrt{C_2(t)}(\mathbf{t}_{2\beta_2}\cdot\mathbf{t}_1)T^2+2C_1(t)(\mathbf{t}_{1\beta_2}\cdot\mathbf{t}_2)T^1, \tag{B13}$$

$$G_1=-\mathbf{w}_{\beta_1}\cdot\mathbf{t}_2-\sqrt{C_2(t)}\mathbf{w}_{\beta_2}\cdot\mathbf{t}_1+2C_1(t)\mathbf{w}_{\beta_2}\cdot\mathbf{t}_2, \tag{B14}$$

$$L_2=\sqrt{C_2(t)}(\mathbf{t}_{1\beta_2}\cdot\mathbf{t}_2)T^1-(\mathbf{t}_{2\beta_1}\cdot\mathbf{t}_1)T^2, \tag{B15}$$

$$G_2=\sqrt{C_2(t)}\mathbf{w}_{\beta_2}\cdot\mathbf{t}_2-\mathbf{w}_{\beta_1}\cdot\mathbf{t}_1. \tag{B16}$$

Define

$$R_1 = L_1 + G_1 + C_1'(t)|\mathbf{z}_{\beta_2}|, \tag{B17}$$

$$R_2 = L_2 + G_2 + C_2'(t)\frac{|\mathbf{z}_{\beta_2}|}{2}. \tag{B18}$$

By differentiating Eqs. (B11)–(B12) with respect to $\beta_1$ and $\beta_2$, we can rewrite the system as

$$\tilde{\Delta} T^3 = \sqrt{C_2(t)}\frac{\partial}{\partial \beta_2}\left( R_1 - \frac{2C_1(t)}{\sqrt{C_2(t)}} R_2 \right) + \frac{\partial R_2}{\partial \beta_1}, \tag{B19}$$

$$\tilde{\Delta} T^4 = \frac{\partial R_1}{\partial \beta_1} - \sqrt{C_2(t)}\frac{\partial R_2}{\partial \beta_2}, \tag{B20}$$

where

$$\tilde{\Delta} = \frac{\partial^2}{\partial \beta_1^2} - 2C_1(t)\frac{\partial^2}{\partial \beta_1 \partial \beta_2} + C_2(t)\frac{\partial^2}{\partial \beta_2^2}$$

is an elliptic operator since $(C_1(t))^2 < C_2(t)$. The right-hand sides are linear functions of $\nabla T^i$ and $T^i$ $(i=1,2)$. The solution exists for (B19), (B20) by the linear elliptic system theory. This completes the derivation of the elliptic system for $T^1$ and $T^2$.

[1] T. S. Lundgren, "Strained spiral vortex model for turbulent fine structure," Phys. Fluids **25**, 2193 (1982).
[2] D. W. Moore, "The spontaneous appearance of a singularity in the shape of an evolving vortex sheet," Proc. R. Soc. London, Ser. A **365**, 105 (1979).
[3] D. I. Meiron, G. R. Baker, and S. A. Orzsag, "Analytic structure of vortex-sheet dynamics. Part 1. Kelvin–Helmholtz instability," J. Fluid Mech. **114**, 283 (1982).
[4] R. Krasny, "A study of singularity formation in a vortex sheet by the point vortex method," J. Fluid Mech. **167**, 65 (1986).
[5] M. J. Shelley, "A study of singularity formation in vortex-sheet motion by a spectrally accurate vortex method," J. Fluid Mech. **244**, 493 (1992).
[6] R. E. Caflisch and O. F. Orellana, "Long-time existence for a slightly perturbed vortex sheet," Commun. Pure Appl. Math. **39**, 1 (1986).
[7] J. Duchon and R. Roberts, "Global vortex sheet solutions of Euler equations in the plane," J. Diff. Eqns. **73**, 215 (1988).
[8] S. J. Cowley, G. R. Baker, and S. Tanveer, "On the formation of Moore curvature singularities in vortex sheets," J. Fluid Mech. **378**, 233 (1999).
[9] T. Ishihara and Y. Kaneda, "Singularity formation in three-dimensional motion of a vortex sheet," J. Fluid Mech. **300**, 339 (1994).
[10] M. Brady and D. I. Pullin, "On singularity formation in three-dimensional vortex sheet evolution," Phys. Fluids **11**, 3198 (1999).
[11] D. W. Moore, "Numerical and analytical aspects of Helmholtz instability in theoretical and applied mechanics," *Proceedings of the XVI ICTAM*, edited by F. I. Niordson and N. Olhoff (North-Holland, New York, 1984), pp. 263–274.
[12] R. E. Caflisch and S. Semmes, "A nonlinear approximation for vortex sheet evolution and singularity formation," Physica D **41**, 197 (1990).
[13] T. Y. Hou and P. Zhang, "Growth rates for the linearized motion of 3-D fluid interfaces with surface tension far from equilibrium," Asian J. Math. **2**, 263 (1998).
[14] L. F. Greengard and V. Rokhlin, "A fast algorithm for particle summations," J. Comput. Phys. **73**, 325 (1987).
[15] C. L. Berman and L. Greengard, "A renormalization method for the evaluation of lattice sums," J. Math. Phys. **35**, 6036 (1994).
[16] G. R. Baker, "Generalized vortex methods for free-surface flows," in *Waves on Fluid Interfaces*, edited by R. E. Meyen (Academic, New York, 1983), pp. 53–81.
[17] G. K. Batchelor, *An Introduction to Fluid Dynamics* (Cambridge University Press, Cambridge, 1970).
[18] D. J. Haroldsen and D. I. Meiron, "Numerical calculation of three-dimensional interfacial potential flows using the point vortex method," SIAM J. Sci. Comput. (USA) **20**, 648 (1998).
[19] E. M. Stein, *Singular Integrals and Differentiability Properties of Functions* (Princeton University Press, Princeton, NJ, 1970).
[20] T. Y. Hou and G. Hu, "A nearly optimal existence result for three-dimensional vortex sheets," Commun. Partial Diff. Eqns. (in press).
[21] S. Wu, "Well-posedness in sobolev spaces of the full water wave problem in 3-D," J. Am. Math. Soc. **12**, 445 (1999).
[22] T. Y. Hou and P. Zhang, "Convergence of a boundary integral method for 3-D water waves," Discrete Contin. Dyn. Syst., Ser. B **2**, 1 (2002).
[23] G. Hu, "Singularity formation in three-dimensional vortex sheets," Ph.D. thesis, California Institute of Technology, 2001.
[24] R. E. Caflisch, N. Ercolani, T. Y. Hou, and Y. Landis, "Multi-valued solutions and branch point singularities for nonlinear hyperbolic or elliptic systems," Commun. Pure Appl. Math. **46**, 453 (1993).
[25] H. Si, "Numerical study of interfacial flow with surface tension in two and three dimensions," Ph.D. thesis, California Institute of Technology, 2001.
[26] T. Y. Hou, Z. H. Teng, and P. Zhang, "Well-posedness of linearized motion for 3-D water waves far from equilibrium," Commun. Partial Diff. Eqns. **21**, 1551 (1996).
[27] We thank Professor O. Bruno for kindly suggesting the idea of proving analyticity of $\beta_1(\beta_2, t)$ as a way to exclude the possibility of the singularity formation along a segment of a one-dimensional curve.